Image Cover Sheet

CLASSIFICATION	SYSTEM NUMBER
UNCLASSIFIED	127363

TITLE

MUSIC AND MAXIMUM LIKELIHOOD USING A REFINED PROPAGATION MODEL: PERFORMANCE COMPARISON FOR RADAR LOW-ANGLE TRACKING

System Number:

Patron Number:

Requester:

Notes:

DSIS Use only:

Deliver to:

National Défense
Defence nationale

UNLIMITED

MUSIC AND MAXIMUM LIKELIHOOD USING A REFINED PROPAGATION MODEL: PERFORMANCE COMPARISON FOR RADAR LOW-ANGLE TRACKING (U)

by

Éloi Bossé, Ross M. Turner and Daniel Brookes

DEFENCE RESEARCH ESTABLISHMENT OTTAWA
REPORT NO. 1122

Canada

January 1992
Ottawa

National Defence / Défense nationale

MUSIC AND MAXIMUM LIKELIHOOD USING A REFINED PROPAGATION MODEL: PERFORMANCE COMPARISON FOR RADAR LOW-ANGLE TRACKING (U)

by

Éloi Bossé and Ross M. Turner
Surface Radar Section
Radar Division

and

Daniel Brookes
Advanced Information Technologies (AIT)

DEFENCE RESEARCH ESTABLISHMENT OTTAWA
REPORT NO. 1122

PCN
011LA

January 1992
Ottawa

MUSIC and Maximum Likelihood Using a Refined Propagation Model: Performance Comparison for Radar Low–Angle Tracking

by

Éloi Bossé, Ross M. Turner, Daniel Brookes

Abstract

The performance of the MUSIC algorithm and many other superresolution methods degrades severely with the highly correlated multipath signals encountered in radar low–angle tracking. This deficiency is overcome by deriving new versions of the MUSIC and Maximum Likelihood (ML) algorithms which use a search vector based on a model of the specular multipath. The performance of these two approaches is then compared with that of the well–known MUSIC algorithm using spatial smoothing. Simulations and experiments at X–band indicate that the use of a specular model combined with an array radar having frequency agility gives much more accurate tracking than do the conventional approaches. The experiments were conducted at Sylt (North Sea), Germany, using corner reflectors mounted on poles inserted in the sea bed; sea conditions varied from sea state one to five.

RÉSUMÉ

La performance de MUSIC et de beaucoup d'autres algorithmes superrésolutifs dégrade rapidement en présence de signaux corrélés tels que rencontrés dans le pistage de cibles rasantes au–dessus d'une surface d'eau. Nous proposons dans ce cas d'inclure un modèle spéculaire de la propagation multivoie. Dans ce rapport nous comparons les deux approches qui utilisent le modèle spéculaire, c'est–à–dire de MUSIC et du Maximum de Vraisemblance contre une approche conventionnelle telle MUSIC utilisant le lissage spatial. A l'aide de résultats expérimentaux et de simulations en bande X, nous démontrons que l'utilisation conjointe d'un modèle spéculaire et d'un réseau d'antennes radar opérant à plusieurs fréquences donne un bon pistage là où les approches conventionelles ne fonctionnent pas. Les expériences ont eu lieu en Mer du Nord (Sylt, Allemagne) dans des conditions de mer variant des états de mer un à cinq. Les cibles étaient des tétraèdres montés sur des poteaux plantés dans la mer.

EXECUTIVE SUMMARY

A research program into high–resolution angle–estimation techniques for radar is ongoing at Defence Research Establishment Ottawa (DREO). The application of prime interest is the estimation of the height of low–flying targets such as sea–skimming missiles. Previously, radar performance has not been satisfactory against low–level threats. Reflections from the sea interfere with the desired direct–path signal and prevent an accurate estimate of target height.

Improved radar tracking techniques have been developed at DREO. These techniques employ modelling of the specular multipath to produce new algorithms for processing the outputs of antenna arrays. These models use a priori information such as knowledge of the target range, height of the radar above the sea and sea state to achieve vastly improved target height tracking in the presence of multipath. This "refined" propagation model has been used with Maximum Likelihood estimation (called Refined Maximum Likelihood or RML) and the MUSIC (MUltiple SIgnal Classification) algorithm (called RMUSIC). The very good performance of RML has been verified by simulations and the use of experimental data collected from smooth sea experiments with beacon signals simulating the radar returns.

Recent experiments at Sylt, Germany, held as part of a campaign of AC/243 Panel III, Research Study Group 8, resulted in the collection of radar data for moderate to high sea states. This data was used to verify that good performance is achievable with a specular propagation model even when significant diffuse multipath is present. Using simulations and experimental data from the Sylt trials, we compared the tracking performance of four algorithms: RML, RMUSIC, MUSIC with spatial smoothing (used to decorrelate the direct path and the reflected signal) and the Fourier Transform. These algorithms were used to process the outputs of an eight–element antenna array used with an Experimental Low–Angle Tracking (ELAT) radar system.

In all cases, algorithms that used the refined propagation model (RML and RMUSIC) performed much better than those that did not. RML produced the best results, accurately tracking a corner reflector mounted on a pole which was inserted in the sea floor at a range of 10 km. With the corner reflector at a height of approximately five metres, errors of about two metres were observed. This accuracy

would significantly improve the tracking performance of fire control radars. However, most fire control radars are not realized with an array feed. Further work is required to evaluate the potential of RML when used with ordinary monopulse fire control radars.

CONTENTS

MUSIC and Maximum Likelihood Using a Refined Propagation Model: Performance Comparison for Radar Low–Angle Tracking

1. INTRODUCTION

The performance of the MUSIC (MUltiple SIgnal Classification) algorithm and many other superresolution methods, degrades severely [1,2] in the highly correlated signal environment encountered in low–angle tracking over the sea. The presence of a strong specular reflection when a target is observed within a fraction of an antenna beamwidth from the sea surface renders the conventional MUSIC ineffective for estimating the angle–of–arrival. Spatial smoothing can be used to modify the spatial covariance matrix but the number of snapshots required to decorrelate the signals becomes enormous [3] when applied to low–angle tracking; here the required resolution can be as high as 0.05 of the antenna beamwidth.

We propose to extend the conventional MUSIC technique by replacing the direction–of–arrival (DOA) search vector ordinarily used with a special search vector based on a refined propagation model. We name the modified algorithm " Refined MUSIC " or RMUSIC. This particular search vector represents the case of coherent two–ray multipath with a priori knowledge of the radar–target geometry. The two rays are linearly dependent and related by a multipath reflection coefficient which depends on many parameters: wavelength, sea state, polarization, and radar target geometry. This, in fact, is an extension of the work by Zoltowski and Haber [4] who use a multi–dimensional search to find the combination of the DOA vectors for the coherent signals. By introducing a priori knowledge on the specular reflection coefficient we reduce the problem to a one–dimensional search.

The idea of a refined propagation model has been used previously but not in the context of the MUSIC algorithm. Sherman (1966) [5] used the a priori knowledge of the specular reflection coefficient in the context of monopulse with a technique named "complex indicated angle". Mermoz (1976) [6] proposed to include some propagation parameters into the DOA vector models. Litva and Rook (1980) [7–8] used a detailed propagation model in an algorithm called Correlation Height Analysis (CHA) to track

low–altitude targets. Turner and Bossé (1987) [9] optimized the use of a priori information on the propagation medium in the context of maximum likelihood (ML) estimation theory; they named the algorithm the Refined Maximum Likelihood (RML) technique. The RML algorithm gave very good results under controlled experiments [10].

In this report, the techniques are described and the performance of the algorithms is evaluated using simulated and experimental radar multipath data for a variety of sea states. We compare the performance of RMUSIC and RML with the performance of the well known technique, MUSIC with spatial smoothing.

In September 1990, experiments were performed at the island of Sylt in Germany overlooking the North Sea. The objective of the measurements was to evaluate the performance of model–based algorithms such as RMUSIC and RML in the presence of multipath for a variety of sea conditions. We used an X–band experimental radar system called Experimental Low–Angle Tracking (ELAT) developed at Defence Research Establishment Ottawa (DREO). The experiments were carried out in various sea conditions with two RF transmitted frequencies of 8.6 and 9.6 GHz. The results are presented here.

The report is organized as follows: Section 2 describes the RML algorithm and Section 3 describes RMUSIC. Section 4 gives the results of simulations and Section 5 presents the experimental results. We use the following notation: matrices are represented by bold upper–case letters, vectors by bold underlined lower–case letter, scalars by both upper and lower italic letters. The superscripts, $\hat{}$, $*$, ^{T}, ^{H}, $\| \ \|$ denote estimate, conjugation, transposition, conjugate transposition, and vector norm respectively. The notation $\mathbb{C}^{M*N}$ signifies a M×N complex matrix.

2. THE RML ALGORITHM

The propagation model used in this paper assumes a medium that is linear, homogeneous, isotropic and frequency invariant (narrow–band). The model considers bipath propagation with only a single reflected ray emanating from a virtual target image. We assume that the targets are located at such a distance from the receiving antenna that the impinging waves can be considered as being planar. We consider a two–way transmission model (radar) and a one–way transmission model (beacon).

The geometry for the beacon model is illustrated in Fig.1 assuming an equivalent flat–earth model with parameters compensated for the effects of the earth's curvature. The noise–free observation model for a signal received at the kth element of an array of K sensors is

$$v_k = Q\ exp(-j\xi R)\ exp\{-j\xi(z_k^2 + h_k^2)/2R\} \times \\ [exp(j\xi h_k z_k/R) + A\ exp(-j\xi h_k z_k/R)] \qquad (1)$$

with $\xi = 2\pi/\lambda$ and where λ is the wavelength, z_k the height of the kth element, R is the target range, h_k is the target height and Q is an unknown complex amplitude due to target characteristics. The complex amplitudes of the direct and reflected rays are simply related by a complex multipath reflection coefficient A at point O (Fig.1). A is determined from the reflection and specular scattering coefficients and divergence factor [11]. Polarization enters the model via the reflection coefficient. All quantities are corrected for the earth curvature and these corrections are different for each element height. Therefore we add the subscript $_k$ to target height h.

The geometry for the radar model is illustrated in Fig.2. We consider four separate propagation paths for each element in the array: direct and reflected signals going from the transmitter to the target, and direct and reflected signals returning from the target to the receiving array. We use small angle approximations to derive the signal received at the kth element of the array:

$$v_k = Q\ exp(-j2\xi R)\ exp\{-j\xi(z_k^2 + h_k^2)/2R\}\ exp\{-j\xi(z_e^2 + h_e^2)/2R\} \times \\ [exp(j\xi h_k z_k/R) + A_2\ exp(-j\xi h_k z_k/R)][exp(j\xi h_e z_e/R) + A_1\ exp(-j\xi h_e z_e/R)] \qquad (2)$$

where z_e and h_e are the transmitter and target heights with respect to the tangent plane at the reflection point, O_1, for the transmitted signal; z_k and h_k are the height of the kth antenna element and that of the target measured with respect to the tangent plane at the reflection point, O_2, for the signal returning from the target; and A_1, A_2 are the complex multipath reflection coefficients at point O_1 and O_2 respectively. All the quantities are corrected for the earth curvature.

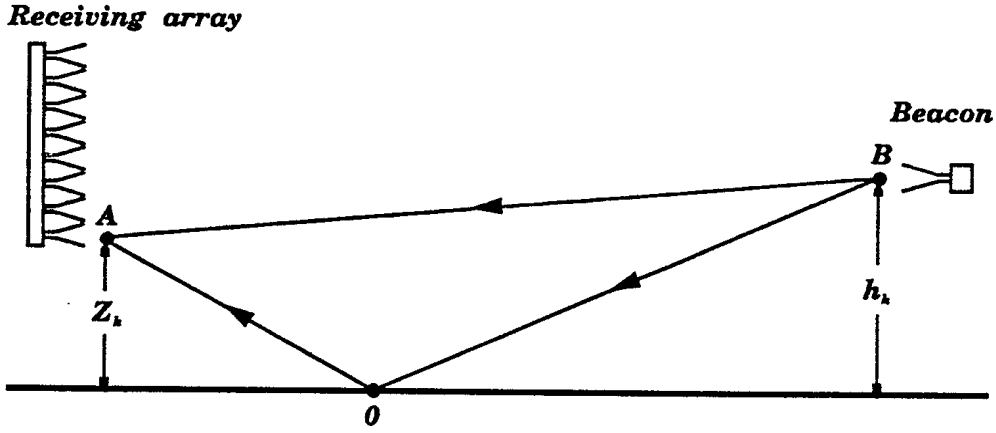

Figure 1 - Geometry for the beacon model

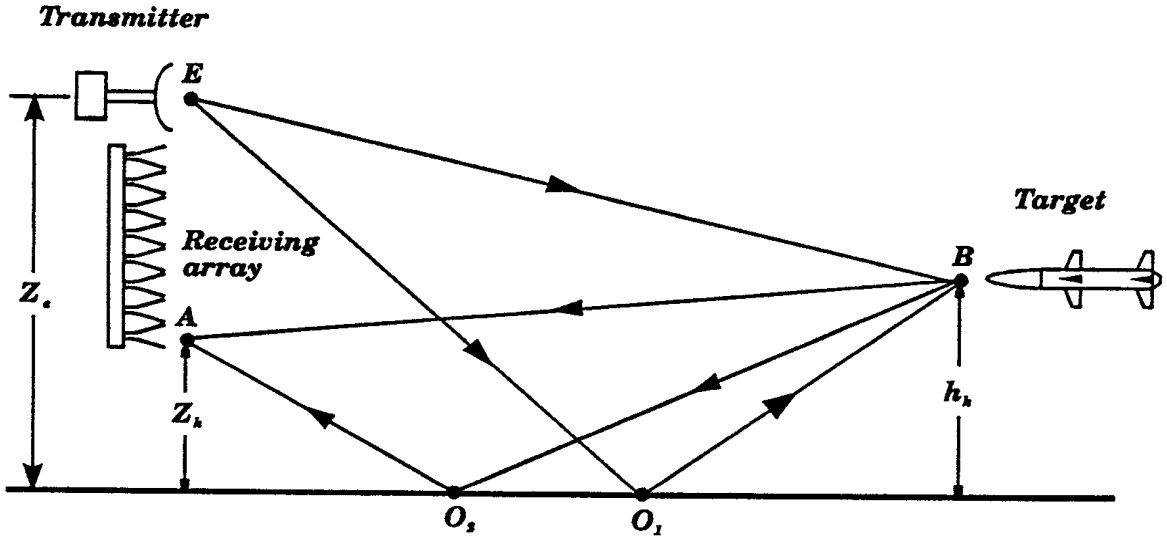

Figure 2 - Geometry for the radar model

To simplify the notation let:

$$v_k = b\, f_k(h) \tag{3}$$

where $$b = Q\ exp(-j\xi R) \qquad \text{(beacon model)} \tag{3a}$$

or $$b = Q\ exp(-j2\xi R)\ exp\{-j\xi(z_e^2 + h_e^2)/2R\} \times [exp(j\xi h_e z_e/R) + A_1\ exp(-j\xi h_e z_e/R)]$$
(radar model) (3b)

and $$f_k(h) = exp\{-j\xi(z_k^2 + h_k^2)/2R\}\ [exp(j\xi h_k z_k/R) + A_2\ exp(-j\xi h_k z_k/R)]$$
(same for both beacon and radar model) (3c)

Assume now that the observation vector or snapshot $\underline{s}$ coming from the output of an array having K sensors is given by

$$\underline{s}_m = b_m\, \underline{f}_m(h) + \underline{n}_m \tag{4}$$

where b_m can be deterministic (non–fluctuating case) or random (fluctuating case) and the noise vector $\underline{n}_m$ is assumed to be stationary, additive, spatially white and independent of the target signals. $(\underline{s}_m,\ \underline{f}_m,\ \underline{n}_m\ ) \in \mathbb{C}^{K*1}$ and $b_m \in \mathbb{C}^{1*1}$. The index m indicates the m^{th} frequency.

In the RML method, "Refined" refers to an improvement obtained by modelling the interference pattern resulting from the summation of a direct path signal and a reflected or image signal. The mathematical description is contained in the model vector $\underline{f}_m(h)$. We treat the information in an optimal way using the ML criterion. We also include frequency agility in the ML optimality criterion; it is an essential requirement for proper functioning of the RML. The height ambiguities arise from the periodicities of the interference pattern. Since the separation of the radar antenna and its image is many wavelengths, the two act as a two–element antenna–array. The resultant pattern has multiple lobes, the number of lobes being proportional to the separation in wavelengths between the radar antenna and its image. The height ambiguities correspond to these grating lobes. Frequency agility is used to resolve these ambiguities.

In this report, we present the first version of the RML technique where the propagation model assumes a medium that is linear, homogeneous, isotropic and frequency invariant (narrow–band). The effects of anomalous propagation, ducting, sea roughness and sea swell are under investigation. We incorporate the effects of surface roughness in the model by decreasing the strength of the specular reflection coefficient according to the experimental work of Beard [15, Fig.2].

The signal model includes only specular reflection; the presence of diffuse multipath superimposed on a specular component leads to model error and biased estimates. It is , in principle, possible to include multipath in the model but this requires a knowledge of the statistics of diffuse multipath: a knowledge that is not available. Nevertheless, in spite of this deficiency, we have obtained good performance for a wide range of experimental conditions ranging from Sea State 0 (SS0) to Sea State 5 (SS5). The results for SS3–SS5, presented in this report, suggest a certain robustness of our technique in the presence of diffuse multipath even though it is not included in the model. However, further experiments are required to confirm those results.

The RML method was introduced by Turner and Bossé [9–10,12]; here, we present only the final result. The RML estimator of the height of a non–fluctuating target (Marcum 0) is the value of h that maximizes the following function:

$$RML(h) = \frac{1}{\sum_{m=1}^{M} \|\underline{s}_m\|^2/\sigma_m^2} \sum_{m=1}^{M} \frac{\|\underline{s}_m^H \underline{f}_m(h)\|^2}{\sigma_m^2 \, \|\underline{f}_m(h)\|^2} \qquad (5)$$

where σ_m^2 is the receiver noise power for the m^{th} frequency.

Fig. 3 shows an example of $RML(h)$ obtained by simulation using the following parameters: a target range of 5 km, a target height of 10 m, a vertical array of 8 sensors equally spaced between 15 and 16 m, and a smooth sea. Fig.3a shows the RML algorithm when m=1 i.e when operating at a single transmitted frequency of 10 GHz. We observe that $RML(h)$ has multiple peaks resulting in height ambiguities as discussed in the previous paragraph. To locate the best estimate of h corresponding to the largest peak, we are forced to make an exhaustive search over a range of height

(a)

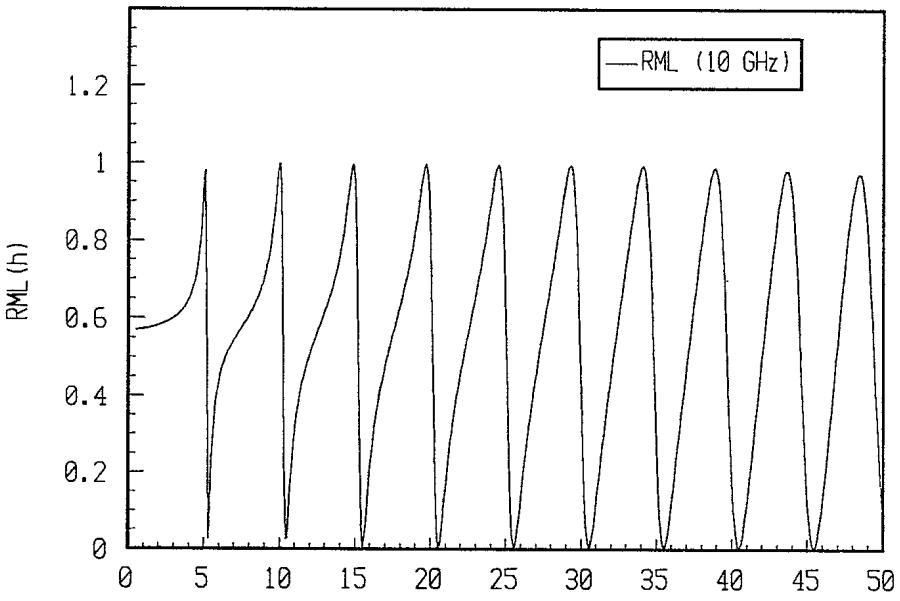

(b)

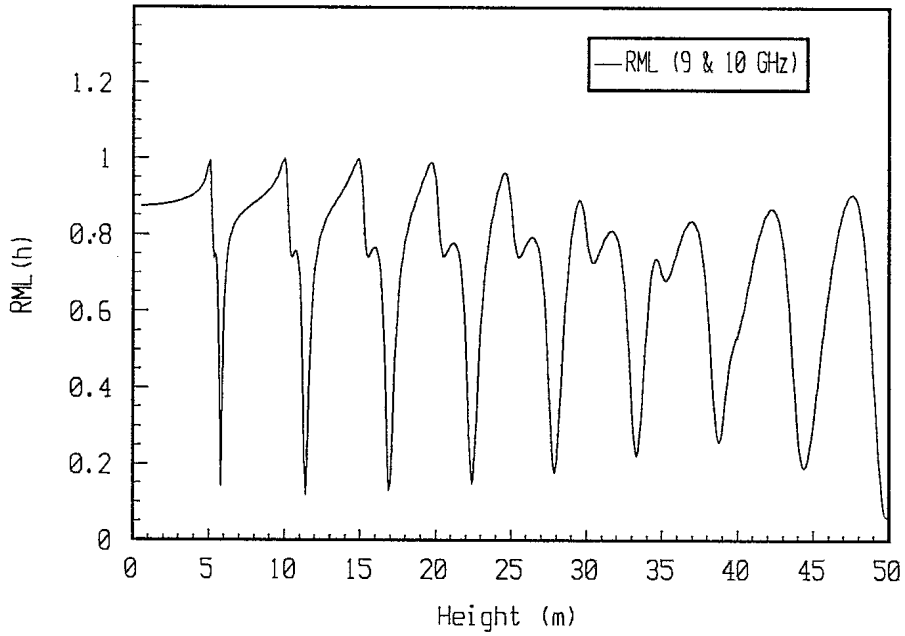

Figure 3: a) An example of RML(h) (single frequency)
b) An example of RML(h) (two frequencies)
(High SNR=100 dB)

values. Since the interference pattern is being detected by an array and the period for the grating lobe repetition is slightly different for each element in the array, the true peak is in theory the largest but the neighboring peaks are so close and the decay in amplitude so slow that amplitude is not a reliable indicator when operating at a single frequency. In Fig.3b, we present $RML(h)$ but this time using two transmitted radar frequencies of 9 and 10 GHz. The use of wide–band frequency agility accentuates the value of the peak corresponding to the true target height relative to the ambiguous peaks. Generally, performance improvement is proportional (perhaps in some nonlinear manner) to the agility bandwidth and the number of frequencies within the band [12].

3. THE REFINED MUSIC (RMUSIC) ALGORITHM

In this section, we use the refined propagation model with the eigenvector methods. Eigenvector methods are based on the properties of the eigenvectors and eigenvalues of the spectral density matrix of the signal received on the array. These properties are asymptotic; therefore, it is necessary to extend results valid for an infinite observation time to a finite observation time. Limitations of resolving power come from limited observation time and discrepancies between the assumed model of the medium and the actual medium. These effects limit the RML method as well.

A representative member of the eigenvector methods is the MUSIC algorithm [13–14]. However, the presence of a highly correlated source, namely the target image, renders the conventional MUSIC ineffective for low–angle tracking over a smooth sea. We propose to extend MUSIC by replacing the direction–of–arrival (DOA) search vector with the refined propagation model vector $\underline{f}_m$; here, the vector $\underline{f}_m$ represents the wavefront shape as sampled by the array geometry when specular multipath is present. In the conventional MUSIC, the DOA vector contains the classical exponentials representing the delay between the signal received by one sensor compared to a reference. In the Refined MUSIC (RMUSIC) the vector $\underline{f}_m$ is the mathematical description of the interaction between the direct and the indirect signals as seen by the array. The presence of height ambiguities leads us to consider the simultaneous use of many frequencies in the bandwidth as in the RML algorithm. Our derivation will follow closely the approach of Bienvenu [15], who has derived the form of the MUSIC estimator for multiple frequencies. This derivation was first given by Bossé and Turner in [16]. Because this reference [16] is not widely known, the derivation is repeated here.

We make the standard assumptions underlying the MUSIC algorithm: stationary processes, known noise covariance matrix, the number of sources, P, less than the number of sensors K, and the number of snapshots greater than the number of sensors. We consider here the case of L snapshots or data vectors taken from a K–element array. The data snapshots are taken at intervals of ℓ=1 to L. We assume that the radar frequency can change from snapshot–to–snapshot, i.e, as a function of ℓ. The case where some or all frequencies are the same is included as a special case of the model. Because, the properties of the eigenvector methods are derived for an infinite observation period, we let $L \to \infty$ in what follows. Performance for a finite L approaches the ideal asymptotically as L becomes large.

We define a single (KL×1) observation vector, $\underline{x}$, which is the concatenation of L (K×1) data snapshots observed at the array output at the intervals, ℓ=1 to L. Corresponding to this observation vector, $\underline{x}$, we define a (KL×1) noise vector $\underline{\xi}$, an (L×1) signal vector, $\underline{v}_i$, for the i^{th} source, i=1 to P sources, and a (KL×L) transfer matrix, $\mathbf{G}_i$, from the signal source to the array outputs. The observation vector is then written as

$$\underline{x} = \underline{\xi} + \sum_{i=1}^{P} \mathbf{G}_i \, \underline{v}_i \tag{6}$$

The deterministic (KL×L) matrix, $\mathbf{G}_i$, is the transfer matrix between the i^{th} source and the signal component of the array output vector, $\underline{x}$. The matrix $\mathbf{G}_i$ contains the directional information on the source positions e.g. the phase delay at the ℓ^{th} snapshot between the source and the array output signals.

The covariance matrix $\mathbf{R}$ is defined as:

$$\begin{aligned} \mathbf{R} &= \mathrm{E}\{\underline{\xi}\underline{\xi}^{H}\} + \sum_{i=1}^{P} \mathrm{E}\{\mathbf{G}_i \underline{v}_i \underline{v}_i^{H} \mathbf{G}_i^{H}\} \\ &= \mathbf{R}_n + \sum_{i=1}^{P} \mathbf{G}_i \, \mathbf{R}_{vi} \, \mathbf{G}_i^{H} \end{aligned} \tag{7}$$

The (L×L) correlation matrix $\mathbf{R}_{vi}$ is Toeplitz since it is a stationary discrete–time stochastic process. The matrix $\mathbf{R}_{vi}$ may be diagonalized by the singular value decomposition (SVD) where the matrix $\mathbf{Q}_{vi}$ that is used to diagonalize $\mathbf{R}_{vi}$ has as its columns an orthonormal set of eigenvectors for $\mathbf{R}_{vi}$. The resultant diagonal matrix,

Λ_{vi}, has as its diagonal elements, the eigenvalues of $\mathbf{R}_{vi}$. We can write

$$\mathbf{R}_{vi} = \mathbf{Q}_{vi}\, \Lambda_{vi}\, \mathbf{Q}_{vi}^{H} \tag{8}$$

It is quite difficult to find analytically the eigenvalues and eigenvectors of a Toeplitz matrix. To circumvent that difficulty we use the fundamental theorem of Szergö [17] on the asymptotic behavior of the eigenvalue distribution of Toeplitz matrices. This theorem relates the properties of Toeplitz matrices to those of circulant matrices. Circulant matrices are an especially tractable class of matrices since the eigenvalues of such matrices can easily be found exactly as the Discrete Fourier Transform (DFT) of their first row and all circulant matrices have the same set of eigenvectors.

The eigenvalues of $\mathbf{R}_{vi}$ are derived by constructing an asymptotically equivalent circulant matrix, $\mathbf{C}_{vi}$ as described in [17]. This is done using two criteria: the strong norm and the weak norm. The strong norm of a (L×L) matrix $\mathbf{R}_{vi}$ is defined as

$$\|\mathbf{R}_{vi}\|^2 = \max_{\underline{x}} \{(\underline{x}^H \mathbf{R}_{vi}^H \mathbf{R}_{vi} \underline{x})/(\underline{x}^H \underline{x})\} \tag{9}$$

and the weak norm of $\mathbf{R}_{vi}$ is

$$|\mathbf{R}_{vi}|^2 = L^{-1}\, tr[\mathbf{R}_{vi}^H \mathbf{R}_{vi}] \tag{10}$$

where the symbol tr means the trace of the matrix which is the sum of its diagonal elements.

The two (L×L) matrices, $\mathbf{R}_{vi}$ and $\mathbf{C}_{vi}$, are asymptotically equivalent if they are uniformly bounded in the strong norm, i.e. there exists a number $M < \infty$ such that $\|\mathbf{R}_{vi}\| \leq M$ and $\|\mathbf{C}_{vi}\| \leq M$, $\forall$ L, and if the measure of the distance, $|\mathbf{R}_{vi} - \mathbf{C}_{vi}|$, between the two matrices approaches zero when $L \to \infty$.

We obtain the eigenvalues of $\mathbf{R}_{vi}$ by taking the DFT of the first row of $\mathbf{C}_{vi}$. Since all circulant matrices have the same set of eigenvectors, the matrices $\mathbf{Q}_{vi}$ all become equal to the (L×L) Fourier matrix $\mathbf{F} = [\underline{\kappa}_1,\ldots,\underline{\kappa}_m,\ldots,\underline{\kappa}_L]$ where the $\underline{\kappa}_m$ vectors are the Fourier vectors . The matrix Λ_{vi} is now a diagonal matrix with elements equal to

the spectral density of signal source i, γ_{im}, for each frequency in the bandwidth. The equation (7) can then be written as:

$$\mathbf{R} = \mathbf{R}_n + \sum_{i=1}^{P} \mathbf{G}_i \, \mathbf{F} \mathbf{\Lambda}_{vi} \mathbf{F}^H \, \mathbf{G}_i^H \tag{11}$$

The matrix $\mathbf{G}_i$ is composed of K square (L×L) matrices $\mathbf{H}_{ik}$. The rows of $\mathbf{H}_{ik}\mathbf{F}$ are the discrete Fourier transform at each frequency m of the rows of $\mathbf{H}_{ik}$. As an example, the m^{th} element of the first row of the k^{th} matrix $\mathbf{H}_{ik}\mathbf{F}$ represents the k^{th} component of the propagation transfer function or DOA vector between the i^{th} source and the various sensors at the m^{th} frequency. At this stage, we introduce the refined propagation model $\underline{f}_{mi}(h)$ used in the RML algorithm to replace the conventional DOA vector. Furthermore, the j^{th} row of $\mathbf{H}_{ik}$ is identical to the first one but delayed by (j–1) samples. The matrix $\mathbf{H}_{ik}\mathbf{F}$ can then be written as

$$\mathbf{H}_{ik}\mathbf{F} = [f_{1ik}(h)\underline{\kappa}_1,\ldots,f_{mik}(h)\underline{\kappa}_m,\ldots,f_{Lik}(h)\underline{\kappa}_L]_{(L\times L)} \tag{12}$$

and the matrix $\mathbf{G}_i\mathbf{F}$ is given by

$$\mathbf{G}_i \, \mathbf{F} = [\underline{\mathbf{f}}_{1i}(h) \otimes \underline{\kappa}_1,\ldots,\underline{\mathbf{f}}_{mi}(h) \otimes \underline{\kappa}_m,\ldots,\underline{\mathbf{f}}_{Li}(h) \otimes \underline{\kappa}_L]_{(KL\times L)} \tag{13}$$

where $\otimes$ means the matrix Kronecker product.

Using eq.(13), the summation part of (11) becomes

$$\sum_{i=1}^{P} \mathbf{G}_i \, \mathbf{F} \mathbf{\Lambda}_{vi} \mathbf{F}^H \, \mathbf{G}_i^H =$$
$$\sum_{m=1}^{L} \sum_{i=1}^{P} \gamma_{im} \, [\underline{\mathbf{f}}_{mi}(h) \otimes \underline{\kappa}_m] \, [\underline{\mathbf{f}}_{mi}(h) \otimes \underline{\kappa}_m]^H =$$

$$\sum_{m=1}^{L} \Gamma_m \otimes (\underline{\kappa}_m \underline{\kappa}_m^H) \tag{14}$$

where Γ_m is the spectral density matrix of the sources at the m^{th} frequency. Explicitly, Γ_m is written as

$$\Gamma_m = \sum_{i=1}^{P} \gamma_{mi}\, \underline{f}_{mi}(h)\underline{f}_{mi}^H(h) \tag{15}$$

Using the assumptions on the noise specified at the beginning of this section, the matrix $\mathbf{R}_n$ is written as

$$\mathbf{R}_n = \mathbf{I} \otimes \Psi_n \tag{16}$$

where Ψ_n is the Toeplitz temporal noise correlation matrix. We proceed the same way as with the signal sources to get

$$\mathbf{R}_n = \sum_{m=1}^{L} \sigma_m^2\, \mathbf{I} \otimes (\underline{\kappa}_m \underline{\kappa}_m^H) \tag{17}$$

and (11) can now take its final form as

$$\mathbf{R} = \sum_{m=1}^{L} [\sigma_m^2 \mathbf{I} + \Gamma_m] \otimes (\underline{\kappa}_m \underline{\kappa}_m^H) \tag{18}$$

To find the eigenvalues and eigenvectors of $\mathbf{R}$ we use the following property of the Kronecker product. If $\{\lambda_i\}$ and $\{\underline{\alpha}_i\}$ are the eigenvalues and the corresponding eigenvectors for the matrix $\mathbf{A}$ and $\{\delta_j\}$ and $\{\underline{\beta}_j\}$ for the matrix $\mathbf{B}$ then $\mathbf{A} \otimes \mathbf{B}$ has eigenvalues $\{\lambda_i \delta_j\}$ with corresponding eigenvectors $\{\underline{\alpha}_i \otimes \underline{\beta}_j\}$ [18]. Applying this property and the fact that the Fourier vectors are orthogonal for different frequencies, we obtain, as in Bienvenu [15] for the conventional approach, (KL) eigenvalues equal to λ_{im} corresponding to the eigenvalues of the matrix $[\sigma_m^2 \mathbf{I} + \Gamma_m]$ and with (KL) corresponding eigenvectors equal to $(\underline{e}_{im} \otimes \underline{\kappa}_m)$.

The derivation of RMUSIC is now straightforward. We use the orthogonality between the vectors $[\underline{f}_{mi}(h) \otimes \underline{\kappa}_m]$ belonging to the source subspace and the eigenvectors $[\underline{e}_{mj} \otimes \underline{\kappa}_m]$ belonging to the orthogonal subspace. The locations of the sources are given by the zeros of the following function:

$$RMUSIC(h) = \sum_{m=1}^{L} \sum_{i=j}^{K} \| \, [\underline{e}_{mi} \otimes \underline{\kappa}_m]^H \, [\underline{f}_{mi}(h) \otimes \underline{\kappa}_m] \, \|^2$$

$$= \sum_{m=1}^{L} \sum_{i=j}^{K} \| \, [\underline{e}_{mi}]^H \, \underline{f}_{mi}(h) \|^2 \tag{19}$$

where j = P + 1, with P and K being the number of sources and the number of sensors respectively.

All the properties used to develop RMUSIC assume an infinite observation time. However in practice, the observation time is limited. In order to compare RMUSIC with RML, the number of frequencies L will be limited to M and both algorithms will be applied to a single target. Therefore the estimate of the target height according to RMUSIC is the value of h that maximizes the following function:

$$RMUSIC(h) = \left\{ \sum_{m=1}^{M} \frac{\underline{f}_m^H(h)[\mathbf{I} - \underline{e}_m \underline{e}_m^H]\underline{f}_m(h)}{\|\underline{f}_m(h)\|^2} \right\}^{-1} \qquad (20)$$

Fig. 4 shows an example of $RMUSIC(h)$ obtained by simulation using the following parameters: a target range of 5 km, a target height of 10 m, a vertical array of 8 sensors equally spaced between 15 and 16 m, 16 snapshots, at a high SNR of 100 dB, and a smooth sea. Fig.4a shows results for the $RMUSIC(h)$ algorithm when m=1, i.e. when operating at a single transmitted frequency of 10 GHz. In Fig.4b, we present results for two transmitted radar frequencies of 9 and 10 GHz. The use of wide–band frequency agility makes the envelope sharper by reducing the amplitude of the ambiguous peaks. Comparing Fig. 4a with Fig.3a, it seems that RMUSIC offers a better discrimination against the ambiguities. However, this is not the case. Fig.4c and Fig.4d show examples respectively for RML and RMUSIC with a low SNR of 4.5 dB. We see that the principal lobe decreases and becomes comparable in size to some of the secondary lobes. Results of Monte–Carlo simulations in Section 4 will show that there is not much difference in performance between RML and RMUSIC although RML gives slightly better performance.

4. RESULTS OF MONTE CARLO SIMULATIONS

We have carried out a preliminary comparative analysis of the RML, RMUSIC and MUSIC using spatial smoothing by means of a Monte Carlo simulation. The simulation is carried out with the same set of parameters as in Fig.3 and Fig.4. The results are presented in Fig.5 where we determine the root–mean–square–error (RMSE) from 200 Monte Carlo trials. The term SNR, in Fig.5, is a per–element

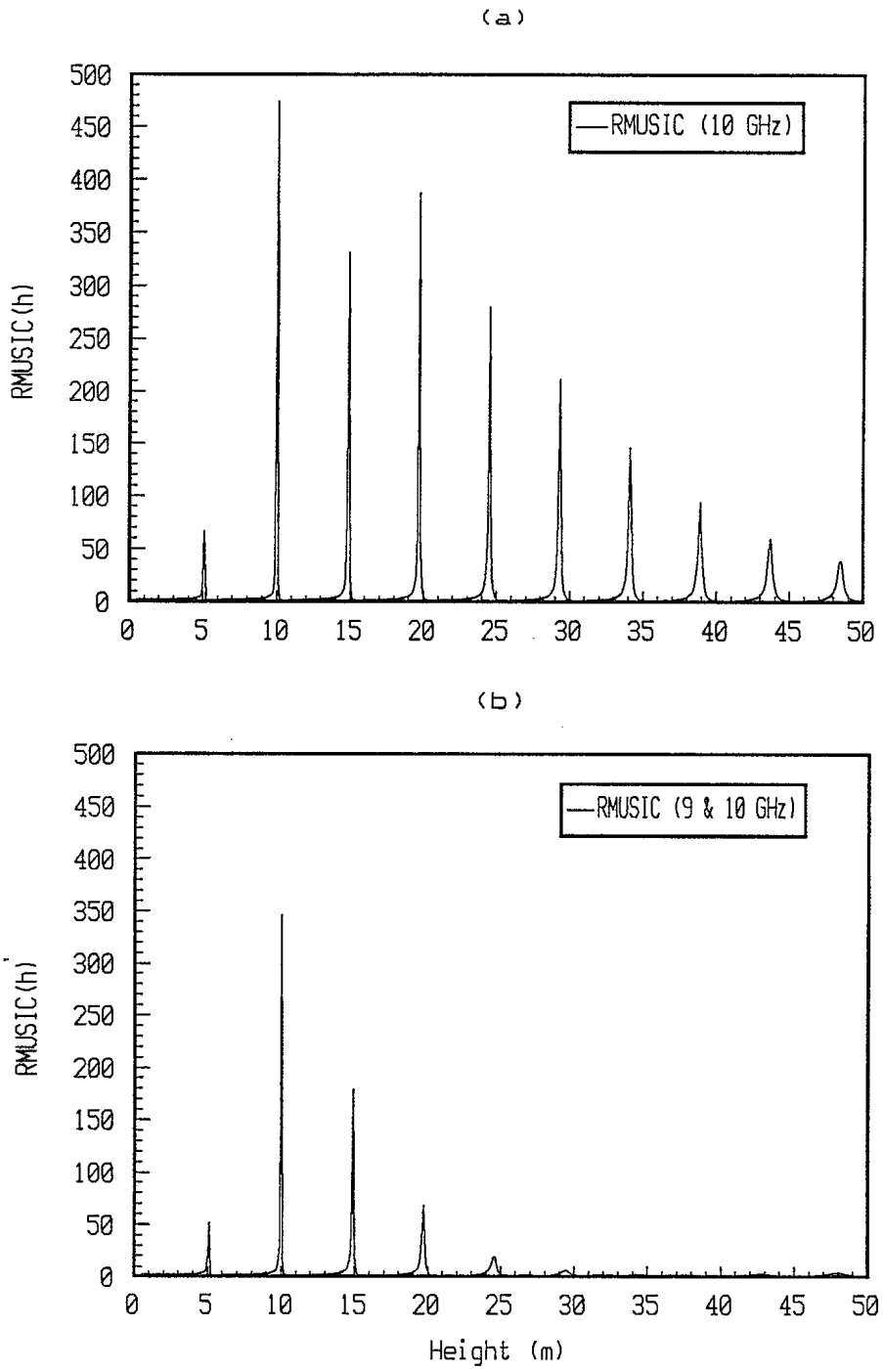

Figure 4: a) An example of RMUSIC(h) (single frequency)
b) An example of RMUSIC(h) (two frequencies)
(High SNR=100 dB)

(c)

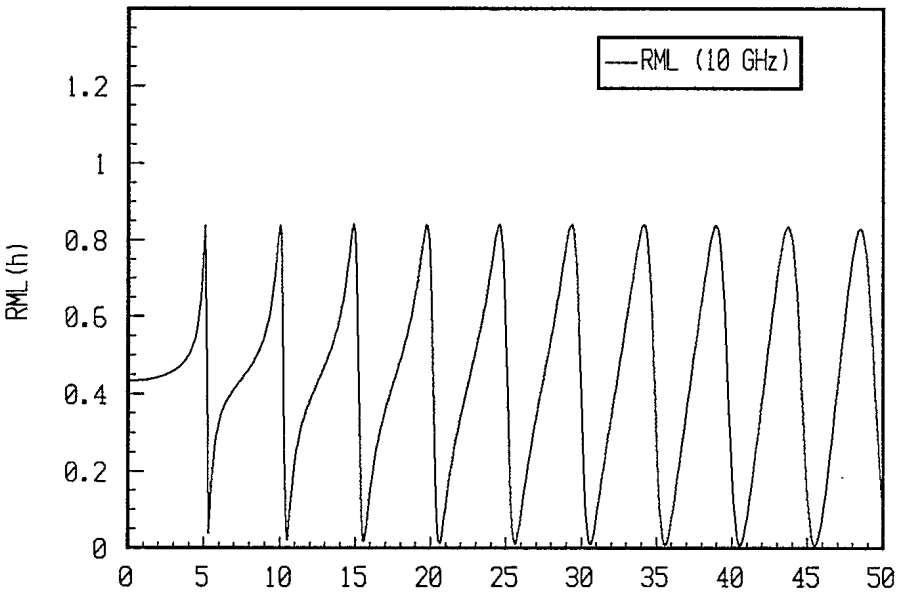

(d)

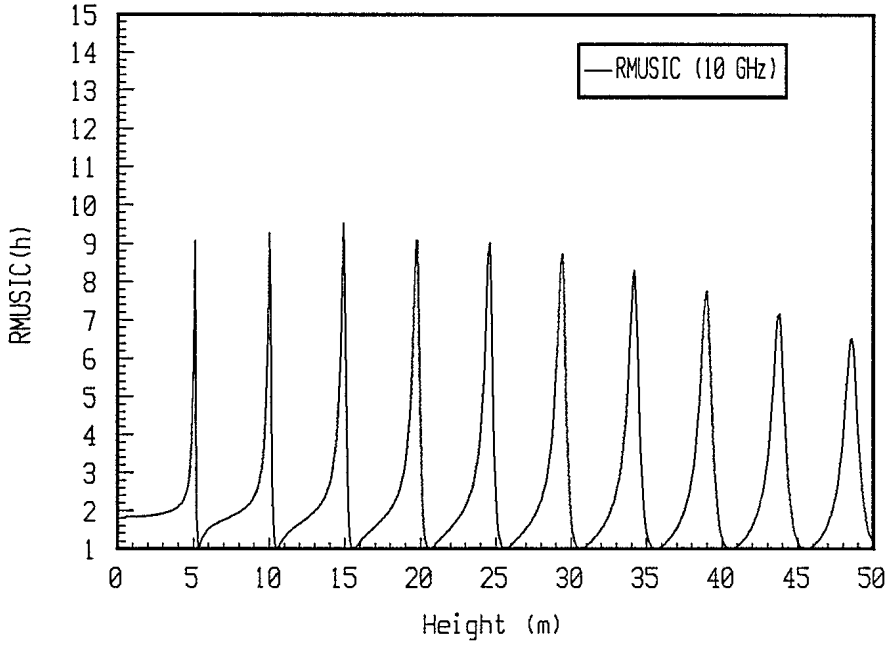

Figure 4: c) An example of RML(h) (single frequency)
d) An example of RMUSIC(h) (single frequency)
(Low SNR=4.5 dB)

signal–to–noise ratio. This term represents the "total" signal–to–noise ratio integrated over all the frequencies as follows:

$$\mathrm{SNR}_{\mathrm{dB}} = 10\ log_{10} \left\{ \sum_{m=1}^{M} \frac{\| b_m \underline{f}_m(h_t) \|^2}{2K\ \sigma_m^2} \right\} \qquad (21)$$

where M is the number of frequencies, h_t= target height and σ_m^2 is the noise power.

In Fig. 5, we present the results for RML, RMUSIC and MUSIC (Spatial Smoothing). The target is at a height of 10 m, a range of 5 km and two frequencies are used: 9 and 10 GHz. RML uses two coherently integrated snapshots, one comprising the integration of 16 snapshots at 9 GHz, the other, the integration of 16 snapshots at 10 GHz. RMUSIC and MUSIC (spatial smoothing) use the 16 snapshots at both frequencies but without coherent integration. In addition, MUSIC (spatial smoothing) breaks up each snapshot into 4 subarrays snapshots by a process of forward–backward smoothing. The results indicate that applying RML on coherently integrated snapshots gives slightly better performance than, obtained from RMUSIC for the same number of snapshots and much better than, obtained from MUSIC with spatial smoothing.

It is well known that one cannot obtain accurate estimates of the target directions with the MUSIC algorithm in case of fully correlated targets. MUSIC (spatial smoothing) circumvents this difficulty by using overlapping subarrays to decorrelate the signals. Unfortunately, the decorrelation effect is weak when the sources are closely spaced in angle. This in turn means that closely spaced, highly correlated, sources can only be resolved if the SNR is very high. The output of each subarray is treated as a snapshot. The decorrelation is accomplished because the phase difference between the target signal changes from subarray to subarray. If the number of elements in the subarray is equal to N_e, the number of subarrays is equal to $2(K-N_e+1)$, where K is the number of sensors and we have used forward–backward subarray smoothing. We have used N_e=7 to obtain the curve labelled MUSIC (spatial smoothing) in Fig.5; this is typical of the best we can obtain using conventional high resolution algorithms on fully correlated signals.

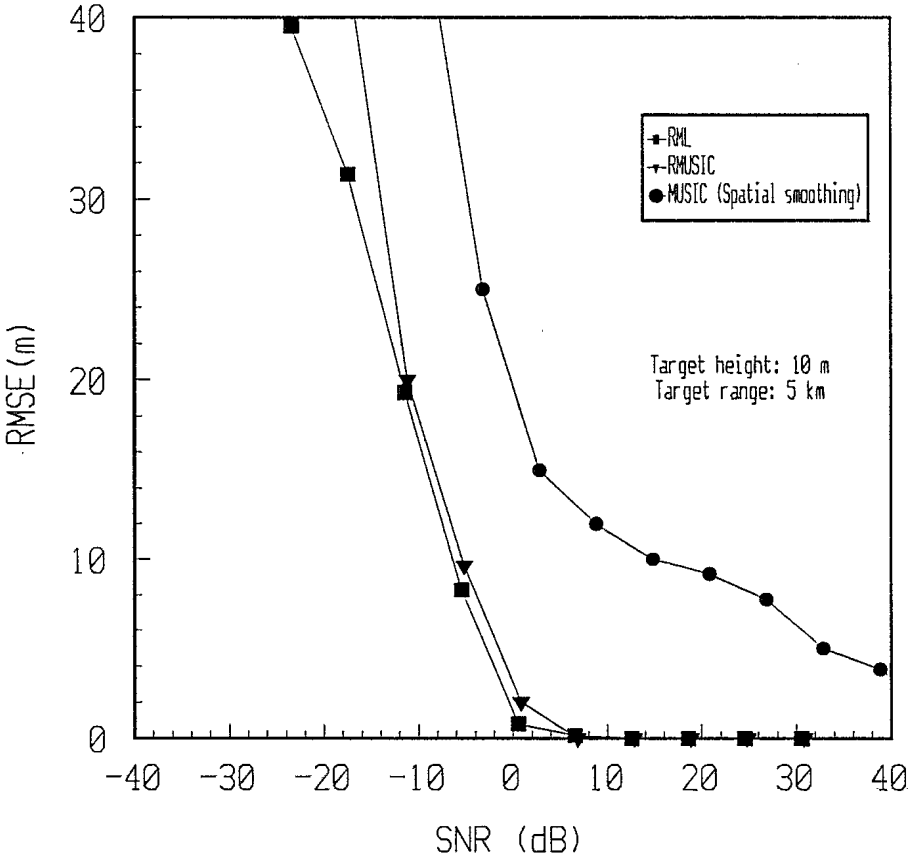

Figure 5: Performance comparison between RML, RMUSIC and MUSIC using spatial smoothing.

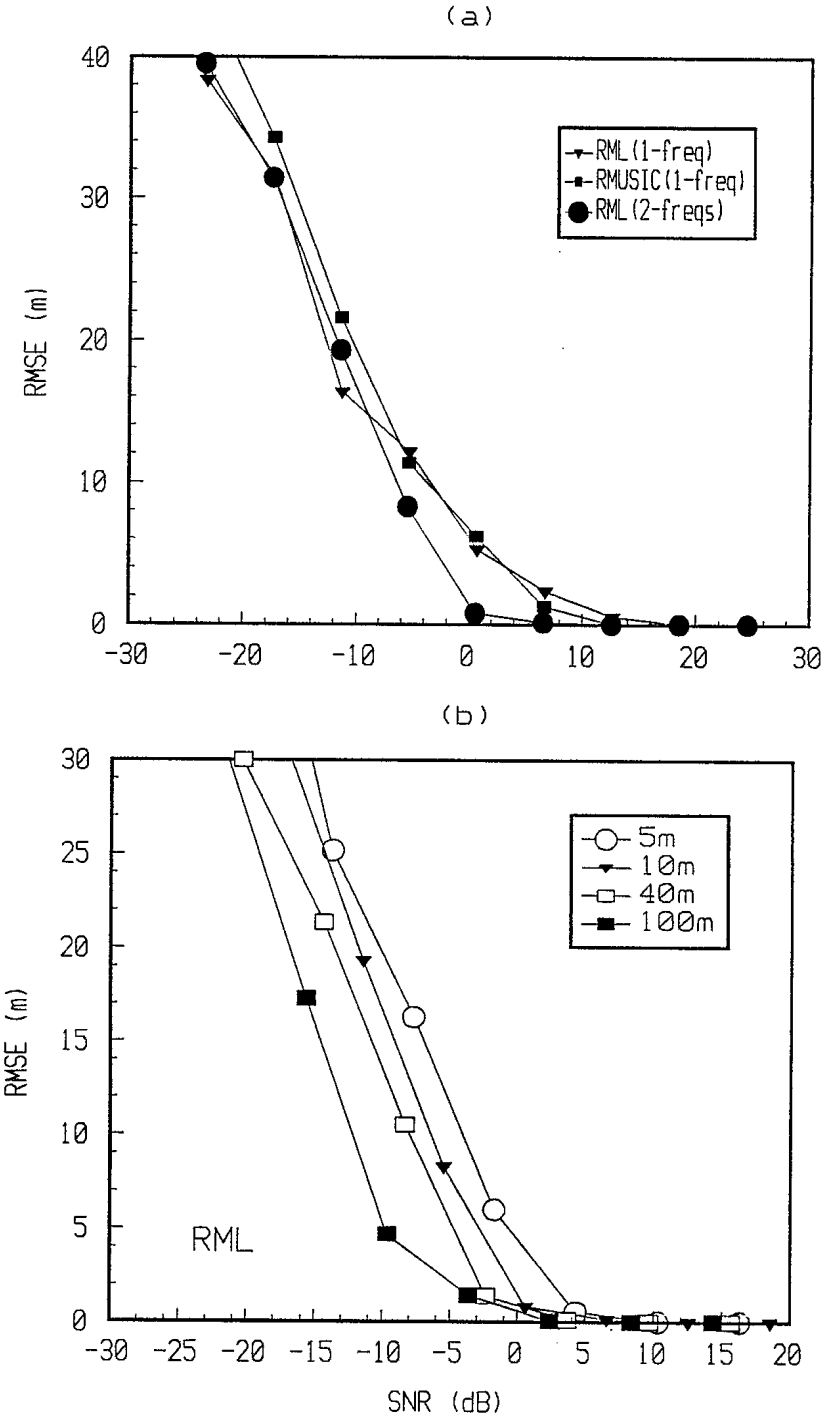

Figure 6:
a) Ambiguities discrimination with RML and RMUSIC
b) Threshold effects for different target heights

In Fig.6a, we compare RML with RMUSIC for one frequency (10GHz) and two frequencies (9 & 10 GHz) for a target height of 10 m and at a range of 5 km. The addition of a second frequency leads to a better discrimination against height ambiguities and therefore to a decrease in the threshold SNR below which, the errors increase rapidly. The two curves labelled RML(1 freq) and RMUSIC (1 freq) in Fig. 6a indicates that both algorithms discriminate similarly against height ambiguities. This result is expected; by modelling the target and its image as one signal, it can be shown [19] that the MUSIC algorithm is a large sample ($L >> 0$) realization of the ML where L is the number of snapshots. The curve labelled RML (2 freq.) shows the improved accuracy gained by adding a second frequency.

In Fig. 6b, we show the performance of RML for target heights of 5, 10, 40 and 100 m at a range of five km using two RF frequencies of 9 and 10 GHz. RML uses the same number of snapshots as in Fig.5. We observe that the performance depends on the separation between the target and its image. The RML algorithm discriminates better against ambiguities for targets at higher altitudes. At very low–angle elevations it may be necessary to increase the number of frequencies and the bandwidth to obtain the same accuracy as at higher altitudes. As an example, the tracking of a target at a height of five meters may required the addition of another frequency and an increase in the bandwidth of one GHz to obtain the same discrimination against ambiguities as obtained for a target at a height of one hundred meters.

For radar low–angle tracking over the sea there are a number of advantages of using the RML algorithm as opposed to the RMUSIC. Both algorithms require pre–processing to remove the sea clutter from the data. Coherent integration is appropriate for RML: clutter is removed, the signal–to–noise ratio is increased and the input data rate to the algorithm is reduced. The RML technique can work with as little as one snapshot in contrast with RMUSIC which requires the number of snapshots to be not less than the number of sensors.

5. EXPERIMENTAL RESULTS

5.1 The Trials Site and Equipment Description:

In September 1990, a series of experiments was performed on the island of Sylt, in northern West Germany. This particular location was chosen because it provides

open sea conditions and the shallow water permits the injection of poles in the bottom of the North sea. Fig. 7 shows the measurement area, with the location of the Experimental Low–Angle Tracking (ELAT) radar; P1 and P2 indicate the locations of the two poles where corner reflectors have been mounted. Fig.8 gives the geometry of the experimental setup.

ELAT was developed at DREO as part of a research program to evaluate alternative techniques for tracking aircrafts and missiles flying low over the sea. The receiver array for ELAT comprises an eight–element vertical array which is illuminated by a cylindrical parabolic reflector antenna as shown in Fig.9. Each element is connected to an individual receiver which carries out a conversion from microwave frequency to the video frequency band. Each receiver includes quadrature (Q) and in–phase (I) detectors which are followed by analog–to–digital converters. Using this receiving arrangement, discrete samples of the electromagnetic field across the vertical antenna aperture can be converted to the video band to form the observation vector or snapshot $\underline{\mathbf{s}}$, used in the various algorithms.

The transmitting antenna is a parabolic antenna designed to floodlight the elevation region of interest. While the elevation coverage of 5.7 degrees is limited, it is quite adequate for proof–of–concept experiments for which the system is designed.

The ELAT radar system is composed of multiple processing units which are dedicated to specific operations such as detection, doppler filtering, digitization, data logging, angle estimation, ...etc. Fig.10 shows a block diagram of the ELAT system. The principal ELAT design parameters are as follows:

Operating range	: 1 km – 15 km
Transmitter type	: Two Magnetrons
Operating frequencies	: 8.6 GHz and 9.6 GHz (X–band)
TX azimuth beamwidth	: 2.4 degrees
TX elevation beamwidth	: 5.7 degrees
TX gain	: 35 dB
RX azimuth beamwidth	: 4.5 degrees
Element elev. beamwidth	: 17 degrees
Polarization	: Horizontal
Number elements	: 8
Element spacing	: 12.5 cm
RX gain	: 25 dB (single element)
PRF	: 0.5K (interleave), 1K (effective) (Hz)
Pulse width	: 1.0 μsec
Peak power	: 65 Kw

5.2 Correction and Calibration of the Data:

Calibration of the antenna array is required to determine the response of each array element. The ELAT receiving array has eight receiving channels; inequalities are present and phase and gain corrections are desirable in order to achieve optimal performance.

The equipment for in situ calibration could not be installed in time for the trials at Sylt. The antenna array suffered progressive deterioration resulting from salt spray to the extent that data taken at the end of the trials were not usable. Therefore it was not possible to measure the correction factors after the trials and we were forced to use data–dependent calibration techniques. We were able to calibrate reasonably accurately for gain variations. Gain calibration was carried out by analyzing a data file which had been collected under very high sea–state conditions – sea state 5 (SS5) in this instance. The sea reflections were essentially diffuse; therefore averaging over many snapshots provided the gain corrections for the array. This was not sufficiently accurate, however, to give the phase corrections.

It is important to note that the introduction of a priori information in the RML method causes a reduction in sensitivity to channel mismatches as compared to standard high resolution techniques. In ref. [20] simulations have been used to measure the effect of channel mismatches on high resolution algorithms. Their principal findings are summarized below. Here $\Delta\phi$ is defined as the phase difference at the middle of the 8–element array between the two signals (target, image).

1) <u>The two–dimensional ML based methods:</u>

– For the special cases when $\Delta\phi = 0$ or 180 degrees phase difference, no amplitude or phase mismatch are tolerable.
– For other cases, $\Delta\phi \neq 0$ and $\Delta\phi \neq 180$ degrees, amplitude mismatches of more than 5% or a phase mismatch of more than 5 degrees cause failure to obtain a proper separation between the target and its image.
– Similar accuracies are required for eigenvector techniques such as MUSIC.

2) The one–dimensional ML–method (RML):

– When $\Delta\phi = 90$ degrees, the RML method is quite robust with respect to both phase and amplitude mismatch. Phase errors up to 20 degrees do not cause significant bias nor do amplitude errors up to 15%.
– When $\Delta\phi = 0$ degrees, the worst case for errors, phase mismatch of 5 degrees and amplitude mismatch of 5% is tolerable.
– When $\Delta\phi = 180$ degrees, phase and amplitude standard deviations of 10 degrees and 10% respectively do not cause bias.
– Values of phase mismatch of 10 degrees and amplitude errors of 10% can be tolerated in the majority of situations.

The results quoted above were obtained using simulations with no receiver noise. In practice, however, the SNR is a determining factor; it is conjectured that the tolerance to calibration errors will decrease as the SNR decreases. A major simulation study is required to establish definitive relationships between SNR and model errors; this is beyond the scope of this report. It is important to realize that the optimum procedure is to apply the calibration information to the model and not to the data, particularly when the SNR changes from one channel to the others. However, when the SNR does not vary from one channel to another, the calibration can be applied to either the data or the model. As this condition was satisfied with the Sylt data, it was more convenient to calibrate the data. The data analysis carried out in section 5.3, made use of calibration data on gain and antenna tilt only.

5.3 Estimation of SNR and Antenna Tilt

The RML algorithm needs the following input parameters:

– Radar receiver height;
– Target range;
– Sea state;
– Antenna array tilt.

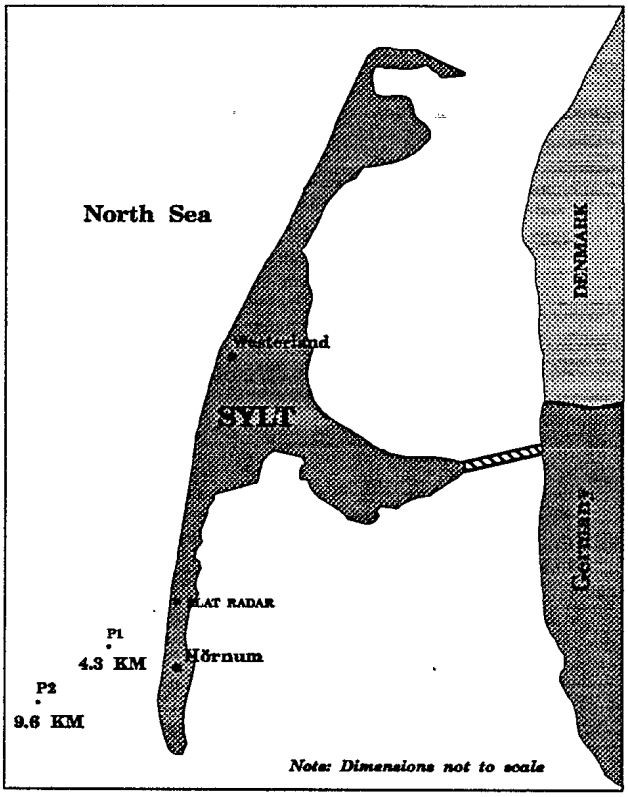

Figure 7 - Geography of the Sylt measurement site.

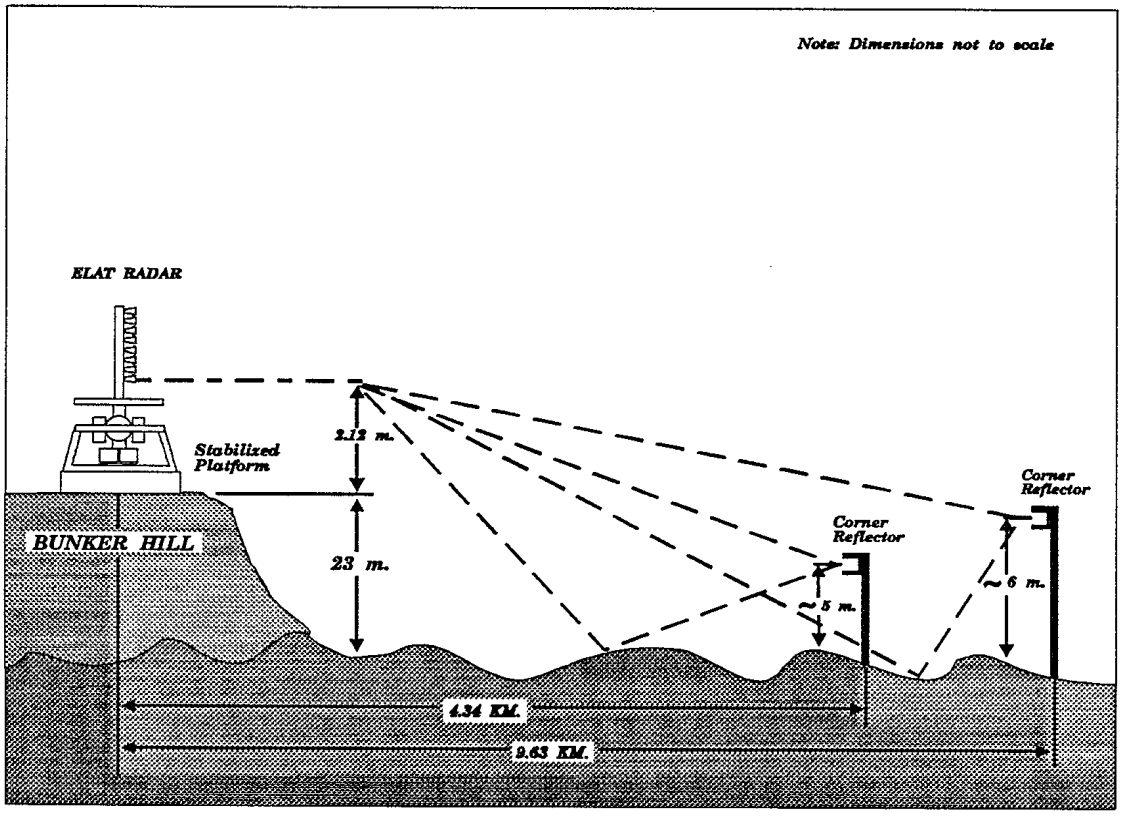

Figure 8 - Geometry of the Sylt experimental set-up.

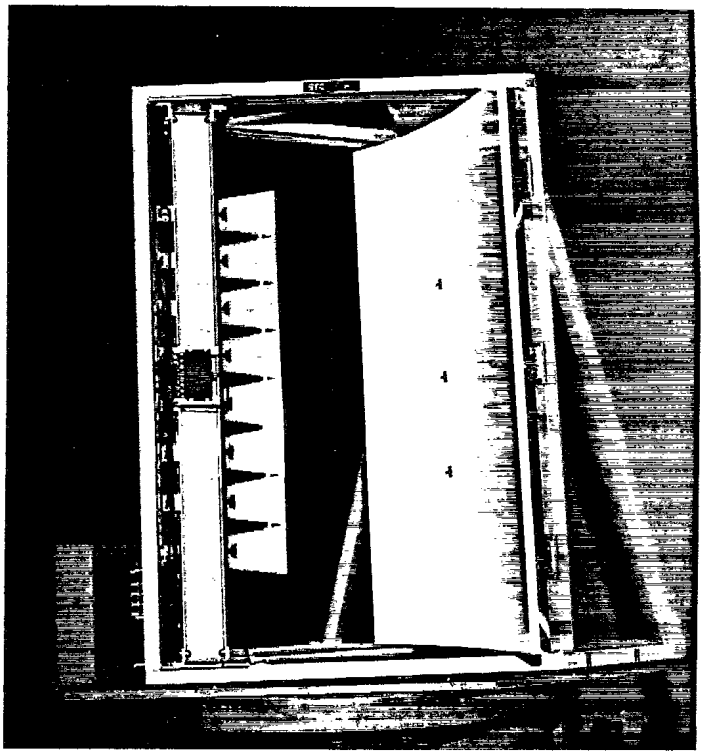

Figure 9: The ELAT receiving antenna array

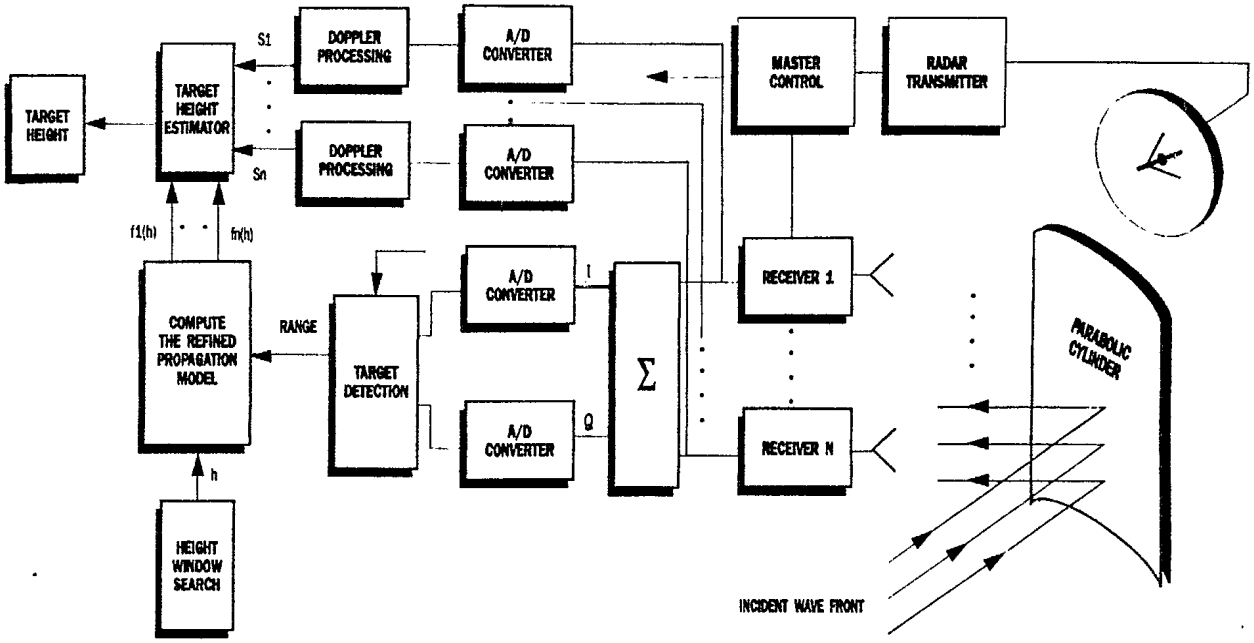

Figure 10: The functional block diagram of the ELAT radar system

To obtain the information required for computing the refined propagation model the ELAT radar (Fig.10) operates in an acquisition mode to determine target range and Doppler velocity. In order to obtain an adequate SNR, 512 data snapshots are coherently integrated prior to use the RML algorithm. The sea state information is given by a wave buoy which provides the Significant Wave Height (SWH).

Unfortunately, we did not collect noise–snapshots only and therefore the SNR must be estimated from recorded data. We use the Fourier Transform. The Fourier vectors form a complete vector space for the experimental data vectors and the noise power is distributed uniformly over all the components of the space. The noise power is estimated by removing from the output of a FFT the Doppler bins corresponding to the signal, the signal image and the clutter and averaging the power over the remaining bins. The SNR indicated on each figure is a per–element SNR. This term is calculated at each frequency and is integrated over the number of frequencies. The amplitude correction is based on the average peak signal from the output of a 512–point FFT.

Fourier beamforming is used to find an initial estimate of the antenna tilt assuming that the image and the pole corner reflector form a composite target at the sea surface. Starting with this initial estimate, the antenna tilt is adjusted till a maximum of correlation is achieved with the RML algorithm. This is, in fact, a maximum likelihood estimate of the antenna tilt. This correction process increases the correlation from about .6 to about .9. Since the correlation function can be no greater than 1.0, this indicates a very good calibration for antenna tilt. For the results presented in Section 5.4, the antenna tilt was found to be .4 degrees.

5.4 Results from the Sylt experiments

This section provides a representative set of results obtained by analyzing data collected with the ELAT radar system at Sylt, Germany. Figures 11–16 present the results for two pole positions, P1 and P2, corresponding to three different sea–state conditions. The figure of merit is how well the various algorithms estimate the known height of a corner reflector mounted on a pole which is projecting out of the sea. Figures 11–15 have plots labelled (a–f) corresponding to the following:

a) The objective function of target height for the RML algorithm (the correlation function between the model and the data) plotted versus target height, h; a peak value close to one indicates a good match between the propagation model and the measured data; the position of the largest peak gives the ML estimate of the target height. Many correlation functions are shown overlapping, each one corresponding to an estimate of the target height.

b) The RML tracking results obtained by estimating height as the position of the maximum in (a).

c) The objective function of target height for RMUSIC, plotted versus h; the functions are superimposed as in (a).

d) Tracking results obtained by using the position of the maximum of RMUSIC(h) as the estimate of height.

e) The objective function of target height for MUSIC, spatial smoothing, plotted versus h with functions superimposed as in (a) and (c).

f) Tracking results for MUSIC, spatial smoothing, with target height estimated from the position of the maxima in (e).

The results are presented for repeated estimates of the height of the pole–mounted corner reflector as indicated by estimate number in (b), (d) and (f) where the dashed line indicates the true height of the corner reflector. The objective functions are plotted superimposed in (a), (c), and (e) to indicate the variation from sample to sample.

Figures 11–13 show the results for RML, RMUSIC and MUSIC, spatial smoothing, for pole P1 at a distance of 4.3 km with three sea–state ranges: SS1–SS2, SS3–SS4, and SS4–SS5. There are thirty estimates for each file corresponding to five minutes of data. It was found that there was a limit to the maximum number of coherently integrated returns. This is attributed to motion of the corner reflector caused by waves and high winds. Therefore we have coherently integrated 512 returns per snapshot and combined non–coherently eight such snapshots in the RML estimator (eq.5). The results for RMUSIC were obtained with eight snapshots, each snapshot consists of 512 coherently integrated radar returns for each of the two RF frequencies, those for MUSIC with spatial filtering use four times as many snapshots counting the expansion by four provided by forward–backward smoothing over four subarrays per full array snapshot.

Figures 11a, 12a, and 13a show the objective function for RML. In the case of RML the objective function is a correlation function having an upper limit of one. The fact that we achieve values close to .9 indicates a good match between the model and the data and a good SNR. The multiple ambiguous peaks require a good SNR to correctly discern which peak is the maximum and to have only a small deviation from the true target height. The estimated per–element SNR (integrated over both frequencies) is 42 dB, 40 dB, and 45 dB for figures 11, 12, and 13. These are quite high and are necessary to obtain target height estimates within the graphic scale for the conventional MUSIC illustrated in Figures 11f, 12f, and 13f. The required SNR for obtaining good tracking performance with the RML algorithm is much lower. This will be discussed later with respect to Figures 17–18. The worst tracking performance was obtained for the lowest SNR as shown in Fig. 12b for an SNR of 40 dB.

The tracking results show a bias; such a bias may be caused by a combination of model and calibration errors. We note however, that the bias for the results for the closer pole P1 are more pronounced than for the further pole P2 where we would expect worse results; i.e., these results are contrary to expectations. We believe this is a result of the fact that the corner reflector for pole P1 was never properly focused on the radar. Pole P2 was focused first and then the arrival of severe storms prevented the focusing of P1. Therefore, it is believed that the corner reflector return from P1 is smaller in comparison to the return from the pole than is the case for P2. This would result in a lower effective height for P1 than for P2. Since the radar tries to measure the effective height, one would expect the estimated height for P1 to be lower in comparison to the true height than is the case for P2 – and this is observed.

The results in Fig.11 correspond to a significant wave height (SWH) of .4 m. For this relatively smooth–sea condition, it is evident that the RML algorithm provides the best and most consistent results. The observed error is equivalent to the separation between adjacent ambiguous peaks of the correlation function or about 1/50 of a beamwidth. It is notable that RML performs slightly better than RMUSIC as indicated by the results of the simulation (Fig.5); this is attributed to the more effective use of coherent integration in RML. Performance of MUSIC, spatial smoothing, is much worse than either RML or RMUSIC; 20 % of the estimates are completely off–scale in Fig.11f. In comparison, ordinary Fourier beamforming performs similarly with 20 % of the estimates that are off–scale (Fig.16b).

Fig. 12 presents results for a more difficult operating environment where the significant wave height was approximately 1.5 m (SS3–SS4). Fifty per cent of the time the RML estimates are very close to the true target height. For the other fifty per cent of the time, errors of 5 to 6 ambiguous peaks occur representing errors of about 1/10 of a beamwidth. RMUSIC and MUSIC, spatial smoothing, do not perform nearly as well as RML.

Fig. 13 presents results for a very rough sea with SWH of 2.3 m (SS5). The target height is obviously lower with respect to the reflecting surface than for a smooth sea. This is reflected in the results of Fig. 13b; all estimates given by RML are below 5 m. Here, RMUSIC gives a performance similar than RML while MUSIC, spatial smoothing, perform worse, having 20 % of estimates off–scale. FFT beamforming (shown in Fig.16f) performed well, likely as a result of the greatly reduced sea reflection.

The results for the more distant pole P2 are presented in Figures 14 and 15. Pole P2 was at a distance of 9.6 km and its corner reflector was properly aimed. Therefore, the effective target height of the pole and corner reflector complex is very near the measured height of the corner reflector. The estimated SNRs were 40 dB for Fig. 14 and 42 dB for Fig. 15.

Fig. 14 gives the results for an SWH of 1.5 m (SS3–SS4) while the results of Fig. 15 were obtained for an SWH of 2.3 m (SS5). The RML results are very good in both cases. RMUSIC performs somewhat worse in in Fig. 14 and about the same in Fig. 15. Results for MUSIC, spatial smoothing, indicate that MUSIC cannot resolve the target from its image for the examples presented in both figures.

Fig. 16 gives the results which were obtained using FFT beamforming with the same examples as in Figs.11–13 for three sea–state conditions: SS1–SS2, SS3–SS4, and SS4–SS5. As expected, the best results were obtained for the very rough sea conditions where the sea reflection was much reduced. These results are representative of what might be expected with a monopulse system.

In Fig.17–18, we try to establish the SNR required to operate in similar conditions such as those described in this report. Figs.17–18 present results obtained at different SNRs for the same data files used for Figs.14–15 respectively. The effect of

noise is twofold: (1) The position of the true maximum is perturbed and (2) the selection of the wrong maximum occurs because of perturbation of the peak heights. The most important cause of errors is, (2) the selection of the wrong peak height. For the results of Fig.17 (SS3–SS4), the correct peak height is selected 75% of the time for a SNR of 19 dB; the correct selection occurs 80% of the time when the SNR is 25 dB. In Fig.18, better results are obtained with a selection of the correct peak height 88% of the time when the SNR is 21 dB in SS4–SS5 conditions.

6.0 CONCLUSIONS

We have carried out a comparative study of performance of four low–angle tracking techniques, RML, RMUSIC, MUSIC with spatial smoothing, and Fourier beamforming. The superiority of RML is evident in all of the examples presented in terms of estimation accuracy and, except for Fourier beamforming, in terms of computational load. RML achieved a height accuracy of approximately 2 m for a corner reflector 5 m above the water at a range of 10 km – an accuracy not achievable with monopulse trackers in the presence of multipath. It is evident however, that RML requires a rather high signal–to–noise ratio in order to choose the correct local maximum of the objective function. It is believed that a wider bandwidth, more frequencies and better calibration would produce a greater difference between ambiguous peaks and thus relax the SNR requirements.

For the experimental data from Sylt, the lowest SNR for the presented results was a per–element SNR of 19 dB leading to a selection of the correct track from the ambiguous tracks, 75% of the time. Adding the integration gain for an eight–element array gives an integrated SNR for the array of 28 dB, much higher than required for detection but feasible in a tracking mode where long periods of coherent integration can be used.

RMUSIC used the same propagation model as RML but failed to work as well. This is directly attributable to the requirement for many snapshots in MUSIC algorithms. Since RML requires only one snapshot per RF frequency, the number of radar returns that can be coherently integrated is many times greater than is possible with RMUSIC, leading to the improved performance of RML. As well, the requirement for coherent processing in many radar systems may render it virtually impossible to collect enough snapshots for RMUSIC or MUSIC. The failure of MUSIC

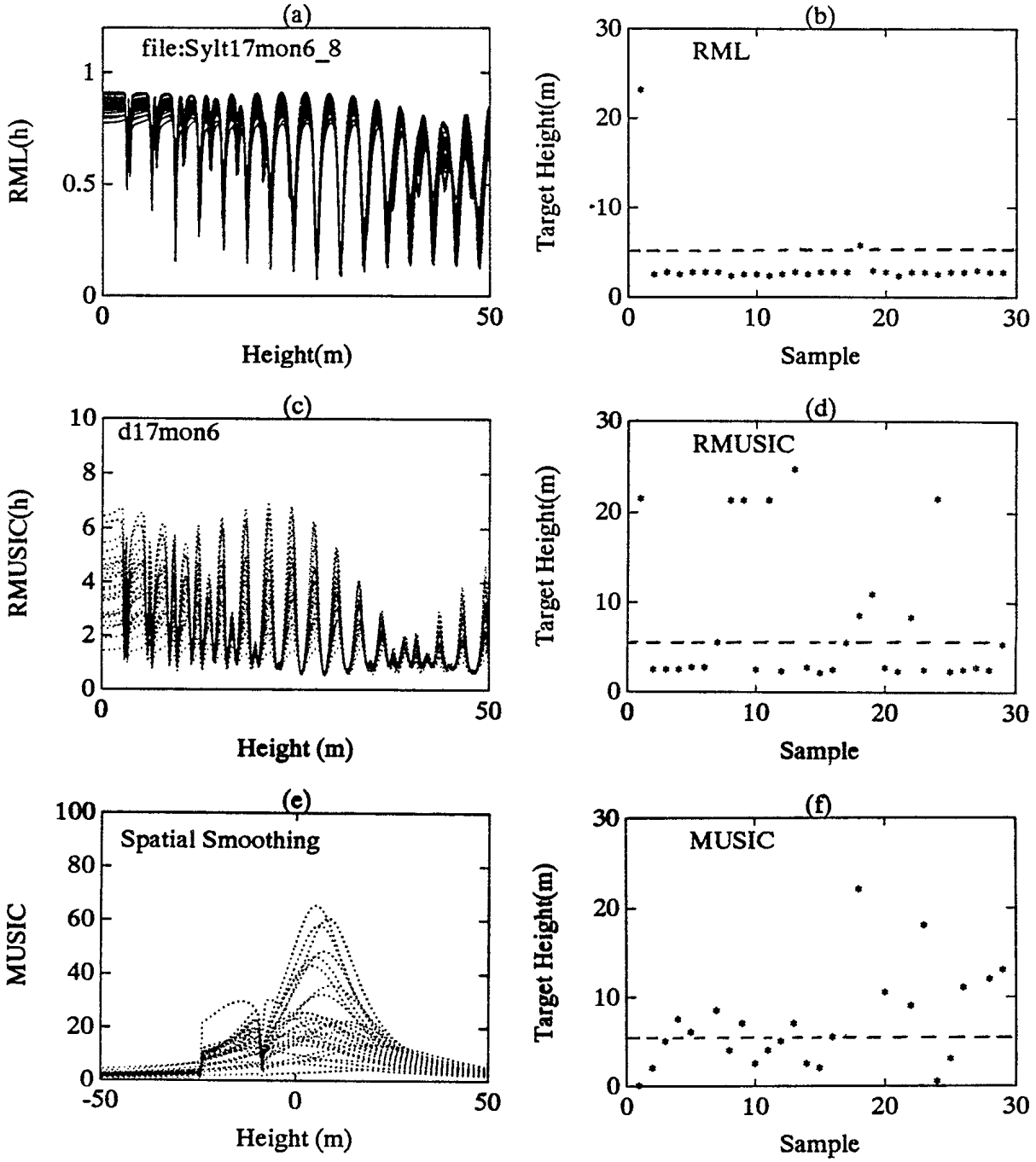

Figure 11: pole P1 (4.3 km) SS1–SS2, SNR = 42 dB

a) The objective function of target height for RML.
b) The RML tracking results.
c) The objective function of target height for RMUSIC.
d) The RMUSIC tracking results.
e) The objective function of target height for MUSIC.
f) The tracking results obtained with MUSIC using spatial smoothing.

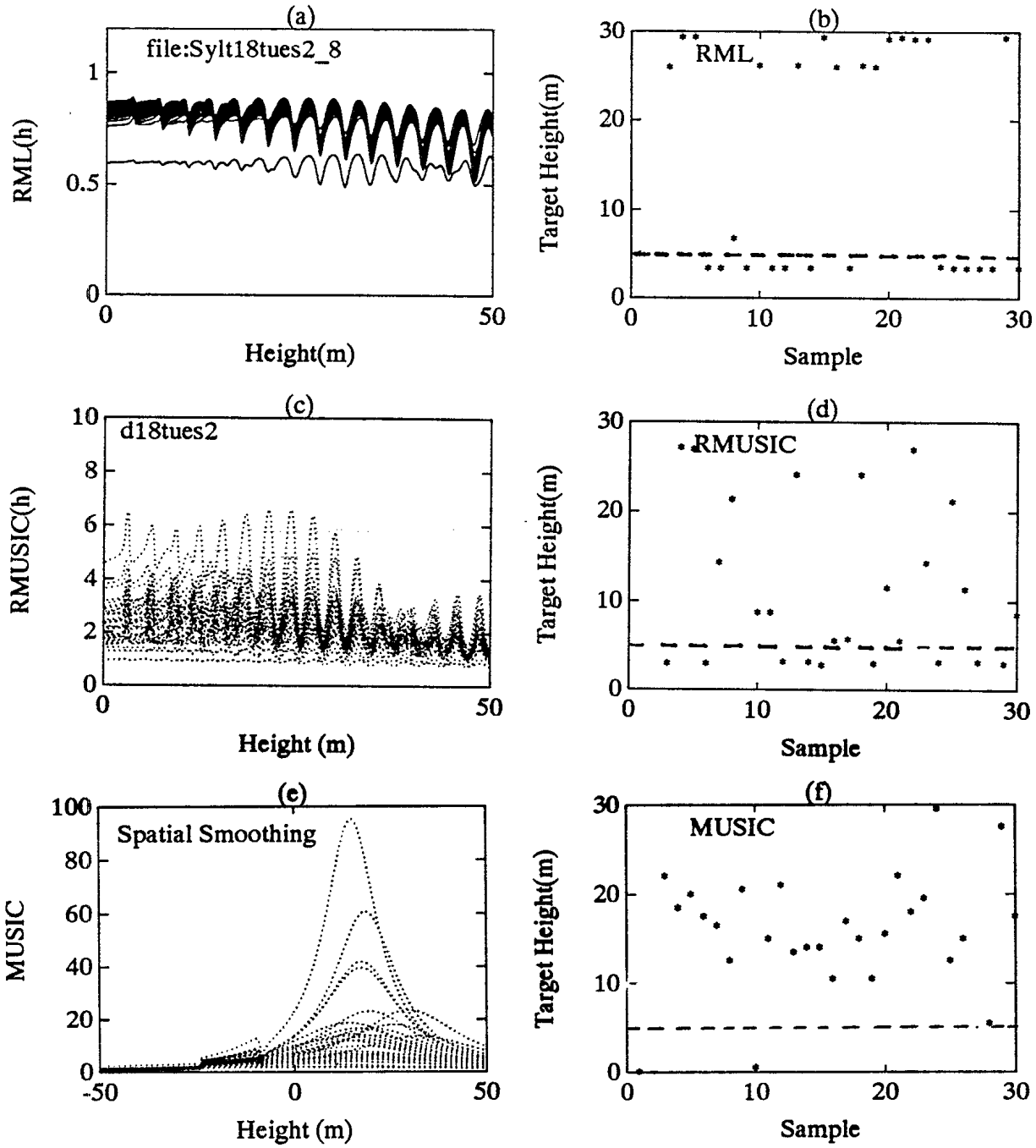

Figure 12: pole P1 (4.3 km) SS3–SS4, SNR = 40 dB

a) The objective function of target height for RML.
b) The RML tracking results.
c) The objective function of target height for RMUSIC.
d) The RMUSIC tracking results.
e) The objective function of target height for MUSIC.
f) The tracking results obtained with MUSIC using spatial smoothing.

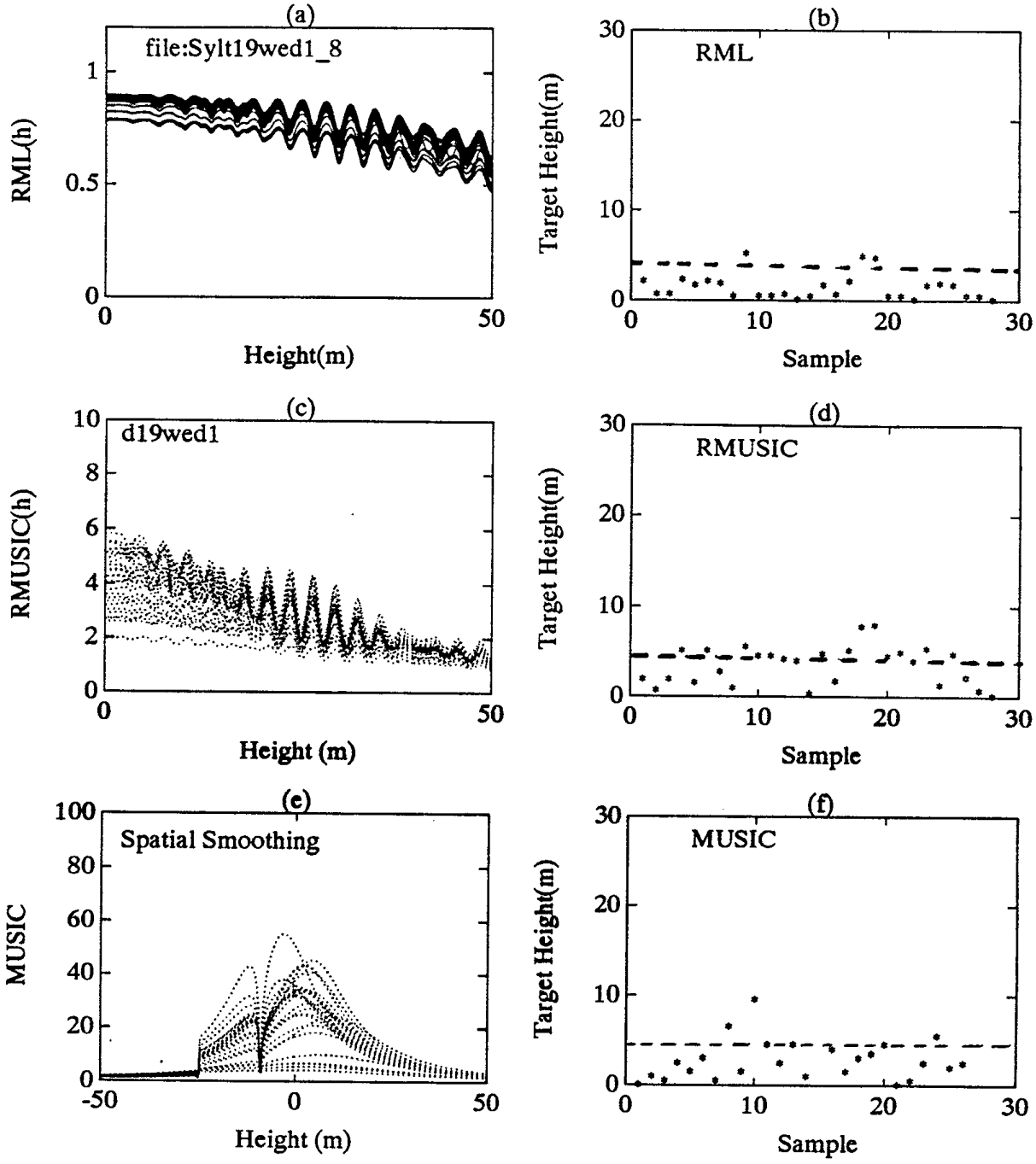

Figure 13: pole P1 (4.3 km) SS4–SS5, SNR = 45 dB

a) The objective function of target height for RML.
b) The RML tracking results.
c) The objective function of target height for RMUSIC.
d) The RMUSIC tracking results.
e) The objective function of target height for MUSIC.
f) The tracking results obtained with MUSIC using spatial smoothing.

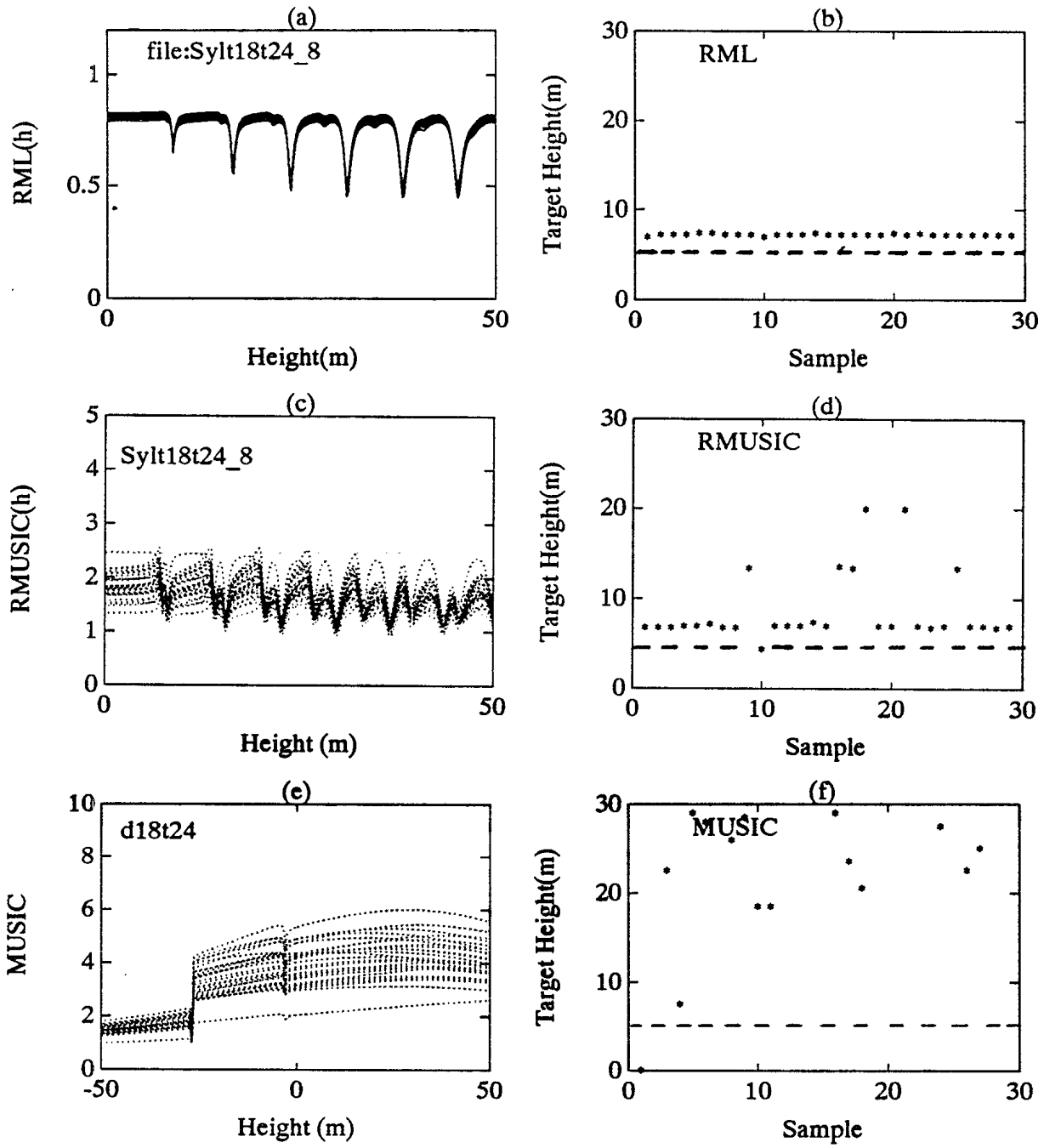

Figure 14: pole P2 (9.6 km) SS3–SS4, SNR = 40 dB

a) The objective function of target height for RML.
b) The RML tracking results.
c) The objective function of target height for RMUSIC.
d) The RMUSIC tracking results.
e) The objective function of target height for MUSIC.
f) The tracking results obtained with MUSIC using spatial smoothing.

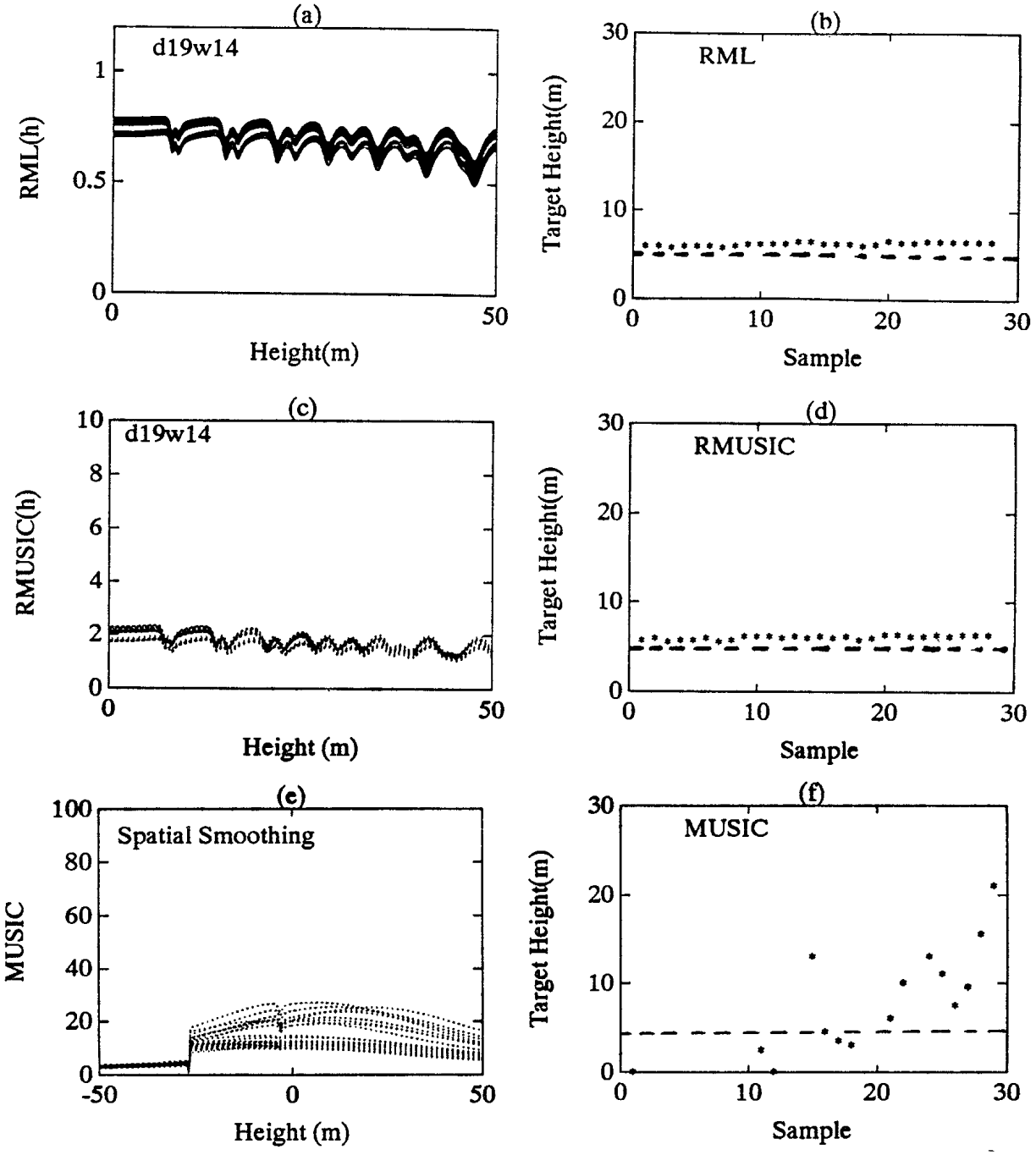

Figure 15: pole P2 (9.4 km) SS4–SS5, SNR = 42 dB

a) The objective function of target height for RML.
b) The RML tracking results.
c) The objective function of target height for RMUSIC.
d) The RMUSIC tracking results.
e) The objective function of target height for MUSIC.
f) The tracking results obtained with MUSIC using spatial smoothing.

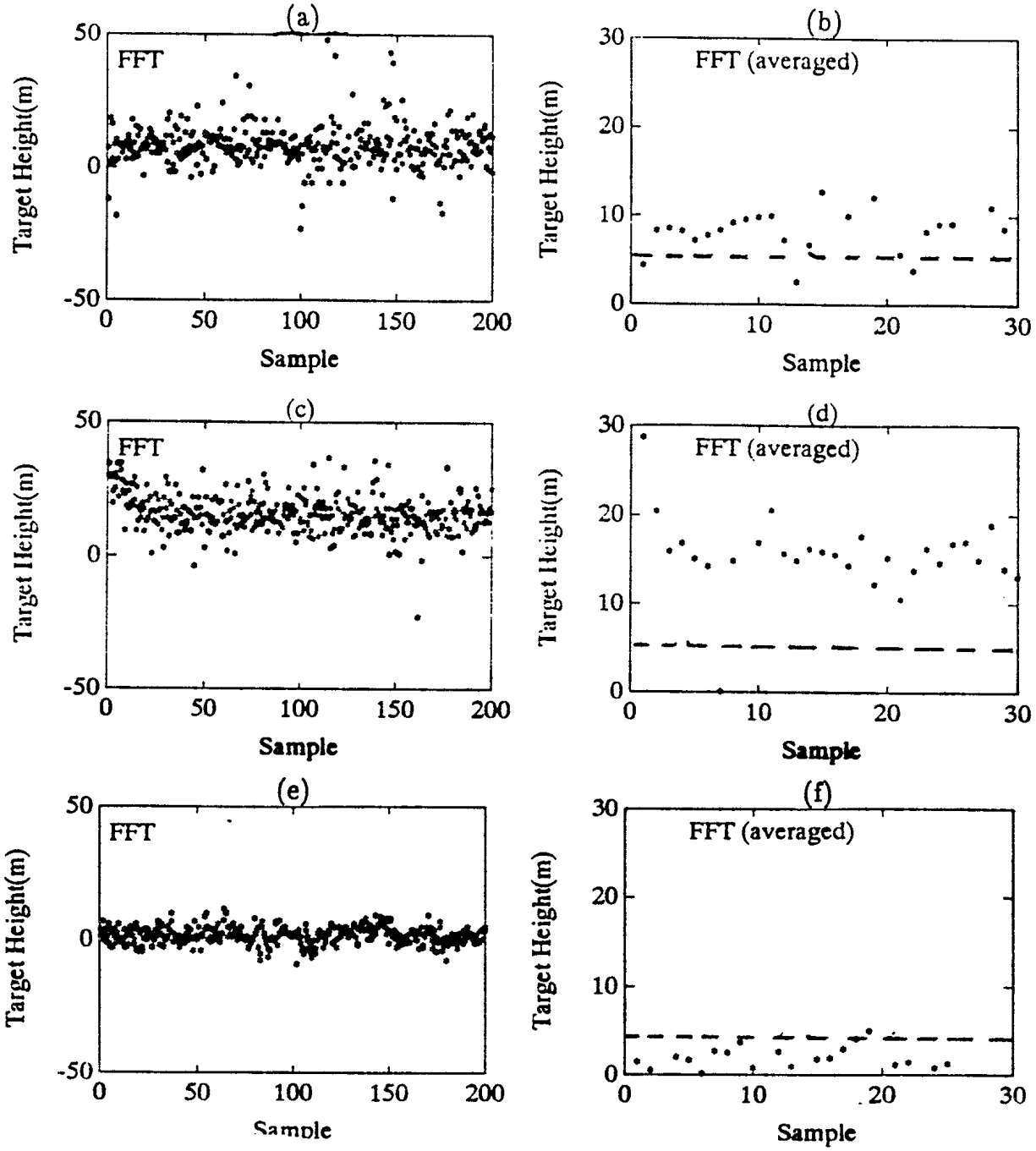

Figure 16: FFT beamforming in different sea–state conditions

a) File:d17mon6, SS1–SS2, single snapshot.
b) File:d17mon6, SS1–SS2, average over 16 target height estimates.
c) File:d18tues2, SS3–SS4, single snapshot.
d) File:d18tues2, SS3–SS4, average over 16 target height estimates.
e) File:d19wed1, SS4–SS5, single snapshot.
f) File:d19wed1, SS4–SS5, average over 16 target height estimates.

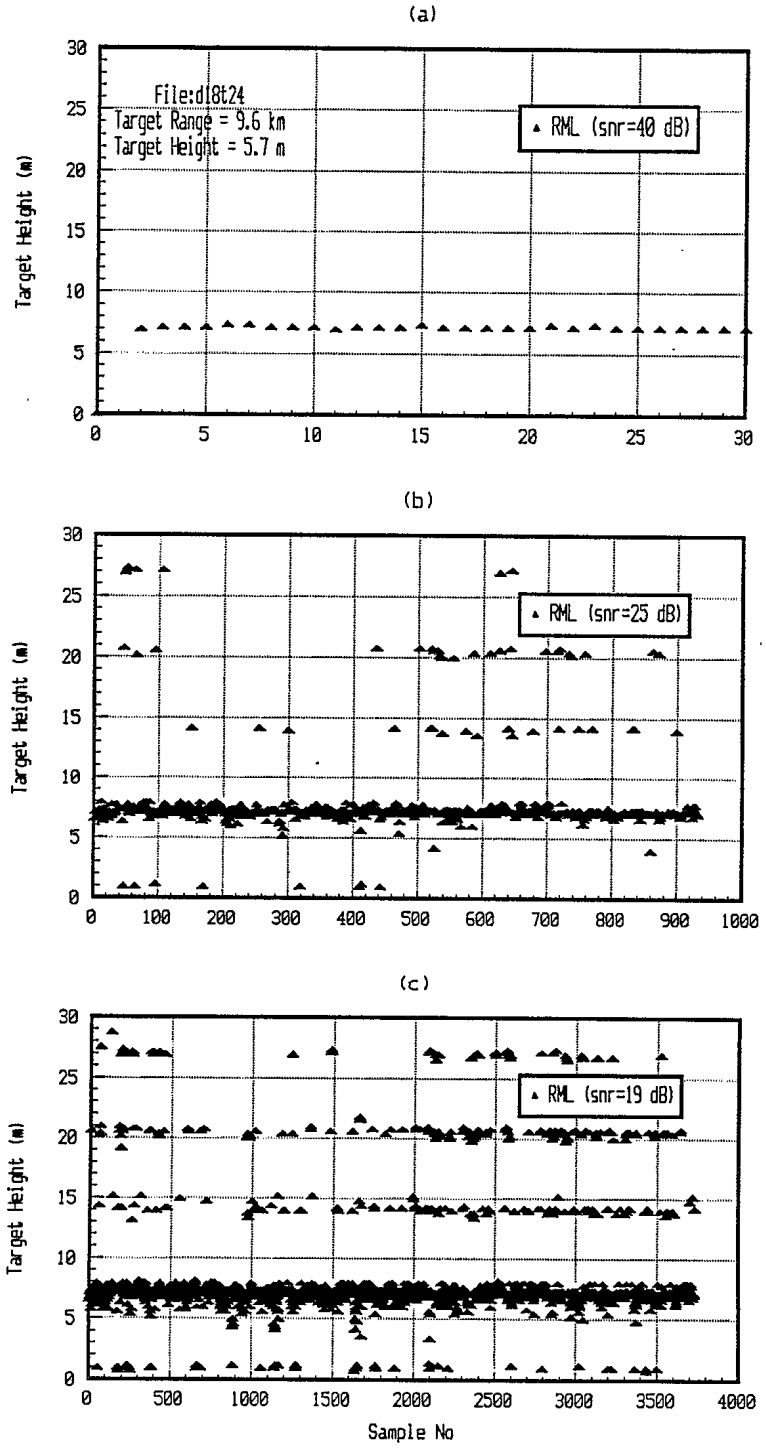

Figure 17: Effect of SNR (SS3-SS4).

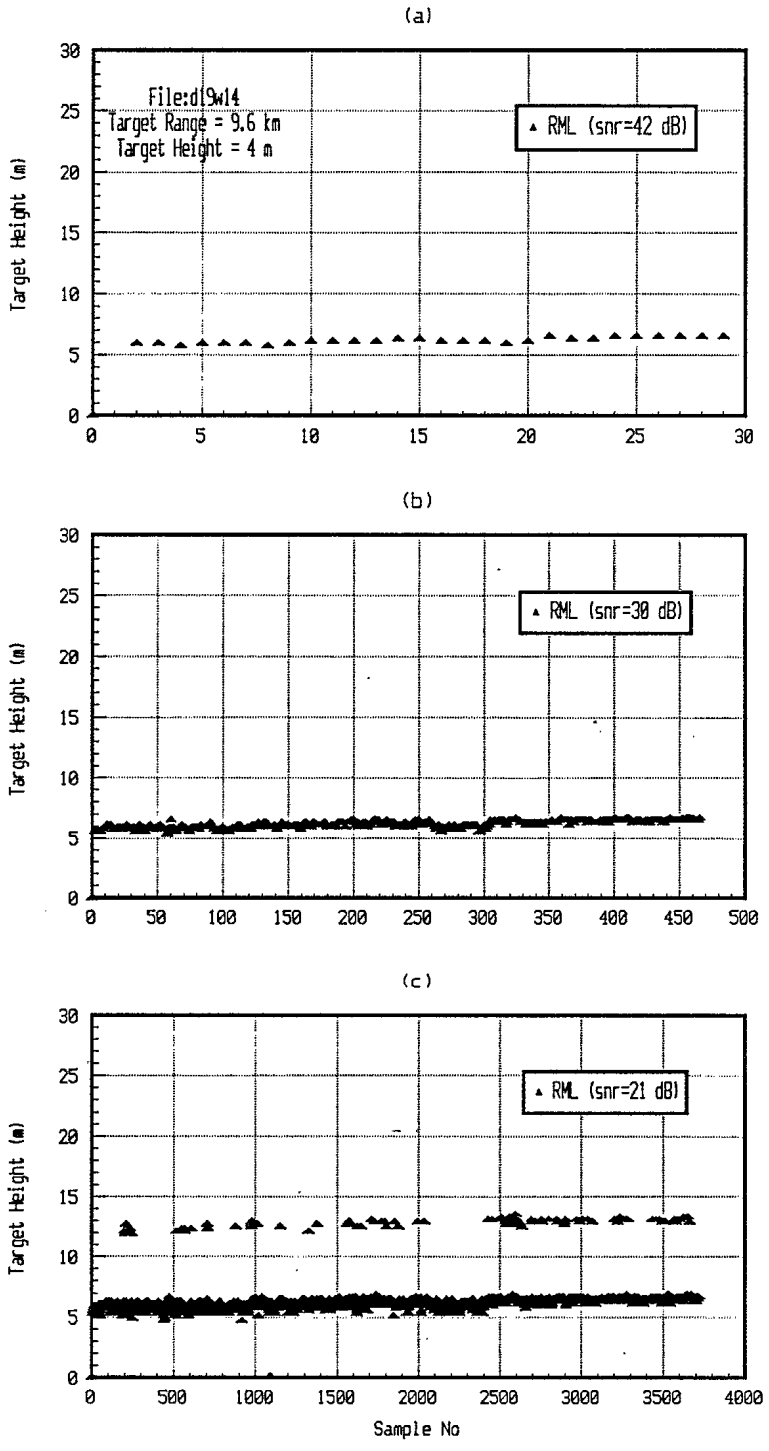

Figure 18: Effect of SNR (SS4-SS5).

with spatial smoothing was expected. The highly correlated direct and reflected signals are much too close in angle–of–arrival to be decorrelated by the moderate amount of spatial smoothing available with an eight–element array. As well, the MUSIC algorithm appeared to be more susceptible to the calibration deficiencies of the array than were any of the other algorithms examined.

7. ACKNOWLEDGEMENTS

The authors acknowledge assistance provided by Ed Riseborough in processing the experimental data as well as the assistance of Denis Lamothe and Applied Silicon Inc. for the collection of the data and for organizing the Sylt Trials. Thanks must also be addressed to Hans Sittrop (FEL/TNO, Netherlands) for providing the information on the target height and sea state.

8. REFERENCES

[1] Evans, J.E, Johnson, J.R, Sun, D.F, " Application of Advanced Signal Processing Techniques to Angle of Arrival Estimation in ATC Navigation and Surveillance Systems", MIT Lincoln Laboratory, Technical Report 582, Lexington, MA, 1982.

[2] Shan, T., Wax, M., Kailath, T., " On Spatial Smoothing for Direction–on–Arrival Estimation of Coherent Signals ", IEEE Trans. ASSP, vol. 33, pp.806–811, Aug. 1985.

[3] Pillai, S.U, " Array Signal Processing ", Springer–Verlag, New–York, pp.132–135, 1989.

[4] Zoltowski, M., Haber, F., " A Vector Space Approach to Direction Finding in a Coherent Multipath Environment", IEEE Trans. on AP, Vol. AP–34, No.9, pp.1069–1079, Sept. 1986.

[5] Sherman, S.M., " Complex Indicated Angles Applied to Unresolved Radar Targets and Multipath", IEEE Trans. on AES, Vol. AES–7, pp.160–170, Jan. 1971.

[6] Mermoz, H., " Imagerie, corrélation et modèles ", Ann. des Télécom., T.31, No.1–2, pp.17–36, Jan.–Feb.1976.

[7] Litva, J., " A New Low–Angle Tracking Technique ", Communications Research Centre, Report No. 1335, Ottawa, May 1980.

[8] Rook, B., Litva, J., " An Improved CHA Algorithm for Tracking Low Angle Targets ", Communications Research Centre, Report No.1356, Ottawa, Jan. 1982.

[9] Turner, R.M, Bossé, E., " Maximum Likelihood Tracking Using a Highly Refined Multipath Model ", 21st Asilomar conference on Signals, Systems and Computers, Pacific Grove, CA, Nov.2–4, 1987.

[10] Bossé, E., Turner, R.M., Lecours, M., " Tracking Swerling Fluctuating Targets at Low Altitude over the Sea ", IEEE Trans. on AES, vol.27, no.5 ,Sept.91.

[11] Kerr, D.E., (ed.), "Propagation of Short Radio Waves", Peter Peregrinus, London, U.K., 1987. (Originally published by McGraw–Hill in 1951).

[12] Bossé, E., Turner, R.M, " Height Ambiguities in Maximum Likelihood Estimation with a Multipath Propagation Model ", 22nd Asilomar Conference on Signals, Systems and Computers, Pacific Grove, CA, Oct. 31–Nov. 2, 1988.

[13] Schmidt, R.O., " Multiple Emitter Location and Signal Parameter estimation ", Proc. RADC Spectral Estimation Workshop, pp.243–258, Rome, NY, 1979.

[14] Bienvenu, G., Kopp, L., " Adaptivity to Background Noise Spatial Coherence for High Resolution Passive Methods ", Proc. IEEE Int. Conf. Acoust., Speech, Signal Processing, pp.307–310, Denver, CO, Apr.1980.

[15] Bienvenu, G., " Propriétés Haute Résolution de la Matrice de Corrélation Spatiale ", Neuvième Colloque sur le Traitement du Signal et ses Applications, pp.239–245, Nice, France, May 1983.

[16] Bossé, E., Turner, R.M., " The Use of Propagation Modelling in MUSIC and Maximum Likelihood for Low–Angle Tracking ", 24th Asilomar Conference on Signals, Systems and Computers, Pacific Grove, CA, Nov. 5–7, 1990.

[17] Gray, R.M., " On the Asymptotic Eigenvalue Distribution of Toeplitz Matrices ", IEEE Trans. on IT, Vol.IT–18, No.6, pp.725–730, Nov.1972.

[18] Graham, A., " Kronecker Products and Matrix Calculus: with Applications ", Ellis Horwood, Chichester, U.K., 1981.

[19] Stoica, P., Nehorai, A., " MUSIC, Maximum Likelihood and Cramer–Rao Bound ", IEEE Trans. on ASSP, Vol. 37, No.5, May 1989.

[20] Theil, A., Huizing, A.G., Otten, M.P.G., " Angle Estimation in a Multipath Environment with an Eight Element Linear Array Operating at 10.5 GHz ", TNO Report No. FEL 1989–15, The Hague, Netherlands, Jan. 1989.

DOCUMENT CONTROL DATA

(Security classification of title, body of abstract and indexing annotation must be entered when the overall document is classified)

1. ORIGINATOR (the name and address of the organization preparing the document. Organizations for whom the document was prepared, e.g. Establishment sponsoring a contractor's report, or tasking agency, are entered in section 8.)

DEFENCE RESEARCH ESTABLISHMENT OTTAWA
3701 Carling Ave., Ottawa, Ontario
K1A 0Z4

2. SECURITY CLASSIFICATION (overall security classification of the document. including special warning terms if applicable)

UNCLASSIFIED

3. TITLE (the complete document title as indicated on the title page. Its classification should be indicated by the appropriate abbreviation (S,C or U) in parentheses after the title.)

MUSIC and MAXIMUM LIKELIHOOD Using a Refined Propagation Model: Performance Comparison for Radar Low-Angle Tracking. (U)

4. AUTHORS (Last name, first name, middle initial)

Bossé, Éloi, Turner, Ross M., Brookes, Daniel.

5. DATE OF PUBLICATION (month and year of publication of document)

January 1992

6a. NO. OF PAGES (total containing information. Include Annexes, Appendices, etc.)

49

6b. NO. OF REFS (total cited in document)

20

7. DESCRIPTIVE NOTES (the category of the document, e.g. technical report, technical note or memorandum. If appropriate, enter the type of report, e.g. interim, progress, summary, annual or final. Give the inclusive dates when a specific reporting period is covered.)

Technical Report

8. SPONSORING ACTIVITY (the name of the department project office or laboratory sponsoring the research and development. Include the address.)

Defence Research Establishment Ottawa, 3701 Carling Ave., Ottawa, Ontario, K1A 0Z4

9a. PROJECT OR GRANT NO. (if appropriate, the applicable research and development project or grant number under which the document was written. Please specify whether project or grant)

011LA

9b. CONTRACT NO. (if appropriate, the applicable number under which the document was written)

10a. ORIGINATOR'S DOCUMENT NUMBER (the official document number by which the document is identified by the originating activity. This number must be unique to this document.)

DREO REPORT 1122

10b. OTHER DOCUMENT NOS. (Any other numbers which may be assigned this document either by the originator or by the sponsor)

11. DOCUMENT AVAILABILITY (any limitations on further dissemination of the document, other than those imposed by security classification)

(X) Unlimited distribution
( ) Distribution limited to defence departments and defence contractors; further distribution only as approved
( ) Distribution limited to defence departments and Canadian defence contractors; further distribution only as approved
( ) Distribution limited to government departments and agencies; further distribution only as approved
( ) Distribution limited to defence departments; further distribution only as approved
( ) Other (please specify):

12. DOCUMENT ANNOUNCEMENT (any limitation to the bibliographic announcement of this document. This will normally correspond to the Document Availabilty (11). However, where further distribution (beyond the audience specified in 11) is possible, a wider announcement audience may be selected.)

UNCLASSIFIED

SECURITY CLASSIFICATION OF FORM

13. ABSTRACT (a brief and factual summary of the document. It may also appear elsewhere in the body of the document itself. It is highly desirable that the abstract of classified documents be unclassified. Each paragraph of the abstract shall begin with an indication of the security classification of the information in the paragraph (unless the document itself is unclassified) represented as (S), (C), or (U). It is not necessary to include here abstracts in both offical languages unless the text is bilingual).

(S) The performance of the MUSIC algorithm and many other superresolution methods degrades severely with the highly correlated multipath signals encountered in radar low–angle tracking. This deficiency is overcome by deriving new versions of the MUSIC and Maximum Likelihood (ML) algorithms which use a search vector based on a model of the specular multipath. The performance of these two approaches is then compared with that of the well–known MUSIC algorithm using spatial smoothing. Simulations and experiments at X–band indicate that the use of a specular model combined with an array radar having frequency agility gives much more accurate tracking than do the conventional approaches. The experiments were conducted at Sylt (North Sea), Germany, using corner reflectors mounted on poles inserted in the sea bed; sea conditions varied from sea state one to five.

14. KEYWORDS, DESCRIPTORS or IDENTIFIERS (technically meaningful terms or short phrases that characterize a document and could be helpful in cataloguing the document. They should be selected so that no security classification is required. Identifiers, such as equipment model designation, trade name, military project code name, geographic location may also be included. If possible keywords should be selected from a published thesaurus, e.g. Thesaurus of Engineering and Scientific Terms (TEST) and that thesaurus-identified. If it is not possible to select indexing terms which are Unclassified, the classification of each should be indicated as with the title.)

Radar Low-Angle Tracking
Angle-of-Arrival Estimation
Multipath Propagation

UNCLASSIFIED

SECURITY CLASSIFICATION OF FORM

JAN 21 1993

NO. OF COPIES NOMBRE DE COPIES	COPY NO. COPIE N°	INFORMATION SCIENTIST'S INITIALS INITIALES DE L'AGENT D'INFORMATION SCIENTIFIQUE
1	1	DAG
AQUISITION ROUTE FOURNI PAR ▶	DREO	
DATE ▶	08 JANUARY 1993	
DSIS ACCESSION NO. NUMÉRO DSIS ▶	93-00115	

DND 1158 (6-87)

National Defence / Défense nationale

PLEASE RETURN THIS DOCUMENT TO THE FOLLOWING ADDRESS:

DIRECTOR
SCIENTIFIC INFORMATION SERVICES
NATIONAL DEFENCE
HEADQUARTERS
OTTAWA, ONT. - CANADA K1A 0K2

PRIÈRE DE RETOURNER CE DOCUMENT À L'ADRESSE SUIVANTE:

DIRECTEUR
SERVICES D'INFORMATION SCIENTIFIQUES
QUARTIER GÉNÉRAL
DE LA DÉFENSE NATIONALE
OTTAWA, ONT. - CANADA K1A 0K2

#127363